NONSPHERICAL VAPOR BUBBLE COLLAPSE

Thesis by

Richard Bruce Chapman

In Partial Fulfillment of the Requirements

For the Degree of

Doctor of Philosophy

California Institute of Technology

Pasadena, California

1970

(Submitted April 2, 1970)

ACKNOWLEDGMENTS

I am greatly indebted to Professor Milton Plesset for his guidance and suggestions during this investigation. I am also grateful to Barbara Hawk, who typed the text, and Cecilia Lin, who prepared the illustrations. As a graduate student, I have received financial support through a National Science Foundation Traineeship, a California State Scholarship, and a Graduate Teaching Assistantship.

TABLE OF CONTENTS

Abstract

Vapor bubble collapse problems lacking spherical symmetry are solved using a method of simulation designed especially for these problems. Viscosity and compressibility in the liquid are neglected. The method of simulation uses finite time steps and features an iterative technique for applying the boundary conditions at infinity directly to the liquid a finite distance from the free surface. Two cases of initially spherical bubbles collapsing near a plane solid wall were simulated, a bubble initially in contact with the wall and a bubble initially half its radius from the wall at the closest point. In both cases the bubble developed a jet directed towards the wall. Free surface shapes and velocities are presented at various stages in the collapses. Velocities are scaled like $\sqrt{\frac{\Delta p}{\rho}}$ where ρ is the density of the liquid and Δp is the difference between the ambient liquid pressure and the vapor pressure. For $\frac{\Delta p}{\rho} = 10^6 \left(\frac{\text{cm}}{\text{sec}}\right)^2 \approx \frac{1 \text{ atm.}}{\text{density of water}}$ the jet had a speed of about 130m/sec in the first case and 170 m/sec in the second when it struck the opposite side of the bubble. Collapse in a homogeneous liquid was simulated for bubbles with nonspherical initial shapes described by the radii $r_s = R_o\left[1 + \frac{1}{10} P_2(\cos\theta)\right]$ and $r_s = R_o\left[1 - \frac{1}{10} P_2(\cos\theta)\right]$ where $P_2(\cos\theta)$ is the second degree Legendre polynomial. Bubble shapes in both cases were close to those predicted by linearized theory. A simple perturbation study of the effect of a small pressure gradient on a collapsing bubble shows that gravity is ordinarily negligible for bubbles initially one cm. in radius or less.

I. INTRODUCTION

A. Topics in Nonspherical Bubble Collapse

The study of the behavior of a bubble in a liquid is greatly simplified by the assumption of spherical symmetry. Following Rayleigh's[1] classical analysis of a problem first solved by Besant, the inviscid collapse of a spherical cavity in a homogeneous, incompressible liquid under a constant ambient pressure, numerous authors have studied the behavior of spherical bubbles under a wide range of conditions. Far less is known about the nonspherical behavior of bubbles. Because problems lacking spherical symmetry have proven too complex for direct analysis, they have been investigated primarily by qualitative reasoning, experiments, and perturbations from spherically symmetric solutions. One result of these studies has been the theory that cavitation damage is caused by the action of liquid jets formed on bubbles near a solid surface[2].

A perturbation study by Rattray[3] suggested that the effect of a solid wall in disturbing the flow during the collapse of an initially spherical bubble could cause the formation of a liquid jet directed towards the wall. Rattray assumed that the bubble was sufficiently far from the wall so that the deviation from spherical symmetry would be small (of order ϵ) over much of the collapse with a predominance of the lower spherical harmonics in an expansion. Both the bubble radius and the velocity potential were expanded in a harmonic series with the assumption of axial symmetry. The coefficients of the n'th harmonic were assumed to be of the order of magnitude ϵ^n. The

resulting solution suggested a reentrant jet for a high degree of deformation. This jet formation was only speculative, however, since it is not unlikely under any circumstance for a series of Legendre functions to display singular behavior near the axis of symmetry when the series is considered outside its range of validity.

The importance of the influence of a solid boundary on bubble collapse as a possible factor in cavitation damage was further emphasized by Plesset[4] who argued that the stresses caused by the collapse and subsequent rebound of a spherical bubble containing a small amount of permanent gas falls off rapidly as the distance from the bubble is increased. These stresses are too small to damage a solid boundary unless the boundary is quite close to the bubble. Thus a solid wall must have an important effect on the collapse of any bubble capable of damaging it.

Experiments by Benjamin and Ellis[5] confirmed that jets form on bubbles collapsing near a solid wall. Large vapor bubbles, generally about one centimeter in radius, were grown from small nuclei by the application of a negative pressure. High speed photographs were taken of these bubbles as they collapsed near a plane solid surface. The ambient pressure was maintained at about 0.04 atm during collapse so that collapse velocities would be reduced to facilitate the photography. These bubbles were nearly spherical as they started collapsing. First they became elongated in the direction normal to the wall; then they tended to flatten and form an inward moving jet on the side of the bubble opposite the wall. From their photographs Benjamin and Ellis estimated the jet speed to be about

10 meters/second. Benjamin and Ellis concluded that since velocities are scaled like the square root of the pressure, the jet speed under atmospheric ambient pressure would be increased by a factor of about five. It should be remarked, however, that the characteristic pressure in this case is not the ambient pressure but the difference between the ambient pressure and the vapor pressure inside the bubble. Because the vapor pressure of water at room temperature is not negligible compared to 0.04 atm., the scaling factor should be greater than five. This problem will be explored more fully in Chapter IV.

Another major topic in nonspherical bubble studies has been the behavior of small asymmetries of a nearly spherical bubble in an infinite, homogeneous liquid. The distortion of the shape of a nearly spherical bubble is commonly expanded in spherical harmonics so that the radius of the bubble is

$$r_s(\theta,\varphi,t) = R(t) + \sum_{n=1}^{\infty} a_n(t)\ Y_n \qquad (I\text{-}1)$$

where Y_n is a spherical harmonic of degree n. For perturbation solutions the coefficients $a_n(t)$ are assumed to be much smaller than the mean radius $R(t)$.

The central problem is the solution of $a_n(t)$ for a given function $R(t)$ and a set of initial conditions. If the problem is linearized, the various harmonics uncouple[6]. The general linearized equation for $a_n(t)$ was solved for bubbles collapsing or expanding under a constant ambient pressure by Plesset and Mitchell[7], who were able to express their solution in terms of the hypergeometric function.

One important result is that as the mean radius collapses to zero, $a_n(t)$ grows in magnitude like $R^{-\frac{1}{4}}$ and oscillates with increasing frequency. Thus even a small asymmetry will become important after the bubble has shrunk sufficiently.

Naudé and Ellis[8] used the theory of Plesset and Mitchell to analyze their experimental study of the collapse of nearly hemispherical bubbles. Using electric sparks, they generated roughly hemispherical bubbles on a plane solid surface and photographed them as they collapsed. Since the solid wall acts as a plane of symmetry, the theory of Plesset and Mitchell is directly applicable.

A perfectly hemispherical bubble would, of course, remain hemispherical as it collapsed and could be described by a spherically symmetric theory such as Rayleigh's. The asymmetry in this case is due to initial asymmetry in shape or velocity rather than the presence of the solid wall. Such bubbles can exhibit a wide range of behavior, depending on the initial conditions, including the formation of a jet on the axis of symmetry. Although the solution of Plesset and Mitchell does not require the lower harmonics to dominate as does Rattray's solution for the collapse of an initially spherical bubble near a plane wall, the assumption that $|a_n| \ll R$ means that the linearized solution cannot be used to describe the jet formed on a nearly hemispherical bubble at the time that it strikes the wall.

The analysis by Naudé and Ellis showed that the distortion in the shape of their bubbles was primarily composed of the second harmonic with a small contribution from the fourth harmonic. No odd harmonics were present, of course, due to the plane of symmetry.

Naudé and Ellis presented the experimental values of $\frac{a_2(t)}{a_2(o)}$ and $\frac{a_4(t)}{a_4(o)}$ over the first half of the collapse $(1.0 > R(t) > 0.5)$. These values agree with the perturbation solution. Since the contribution from the second harmonic was fairly large, Naudé and Ellis had to add the second order effect of $a_2(t)$ on $a_4(t)$ to obtain close agreement in the fourth harmonic. This second order effect was solved using an assumption analogous to Rattray's, that the lowest harmonic was dominant.

Because the photographic techniques used so effectively by Benjamin and Ellis had not yet been developed, it is not possible to observe jetting directly from the photographs of Naudé and Ellis. They were able to produce some pitting in soft aluminum, however. Similar experiments by Shutler and Mesler[9] also produced pitting. Shutler and Mesler concluded that jets formed but were too weak to cause the pitting which they attributed to rebound bubbles. These results were later challenged by Benjamin and Ellis.

B. Numerical Simulation of Bubble Collapse

The advantages of a numerical technique for simulating non-spherical bubble collapse are clear. Experiments are difficult and give only sketchy results. Perturbations from spherically symmetric solutions are not valid for large deformations. A numerical solution, however, can check results and supply detailed information. Numerical methods can also be applied to situations which might be very difficult to produce in the laboratory.

Attempts to apply the well-known Marker-and-Cell or MAC

technique to nonspherical bubble collapse have not yet been successful. A report by Mitchell, Kling, Cheesewright, and Hammitt[10] considers the feasibility of using the MAC method for this purpose. Before this report is discussed, the MAC method will be briefly described.

The Marker-and-Cell technique is a general method for simulating incompressible, viscid flows with an assortment of boundary conditions including free surfaces. In practice it has been applied only to two-dimensional problems, either plane or axially symmetric flows. The basic calculations are Eulerian. A domain in the two-dimensional Eulerian space is covered by a grid of rectangular cells. The pressure and the velocity are assumed to be nearly constant over a single cell. The pressure distribution is specified by its value at the center of each cell. The horizontal velocity u and the vertical velocity v are specified at the midpoints of the vertical and horizontal sides of each cell, respectively, as illustrated in Fig. 1.

The pressure and the two components of velocity are related through the continuity equation and the two components of the equation of motion. These three equations can be combined to give an expression for the Laplacian of the pressure as a function of the components of the velocity and their first and second space derivatives. In the plane flow case, for example,

$$\frac{1}{\rho} \nabla^2 p = \frac{\partial^2 u^2}{\partial x^2} + 2 \frac{\partial^2 uv}{\partial x \partial y} + \frac{\partial^2 v^2}{\partial y^2} \quad . \tag{I-2}$$

For the finite difference approximation to this equation and other details concerning the MAC method reference may be made to

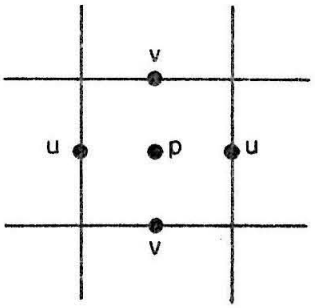

Fig. 1 Cell Used by the MAC Method

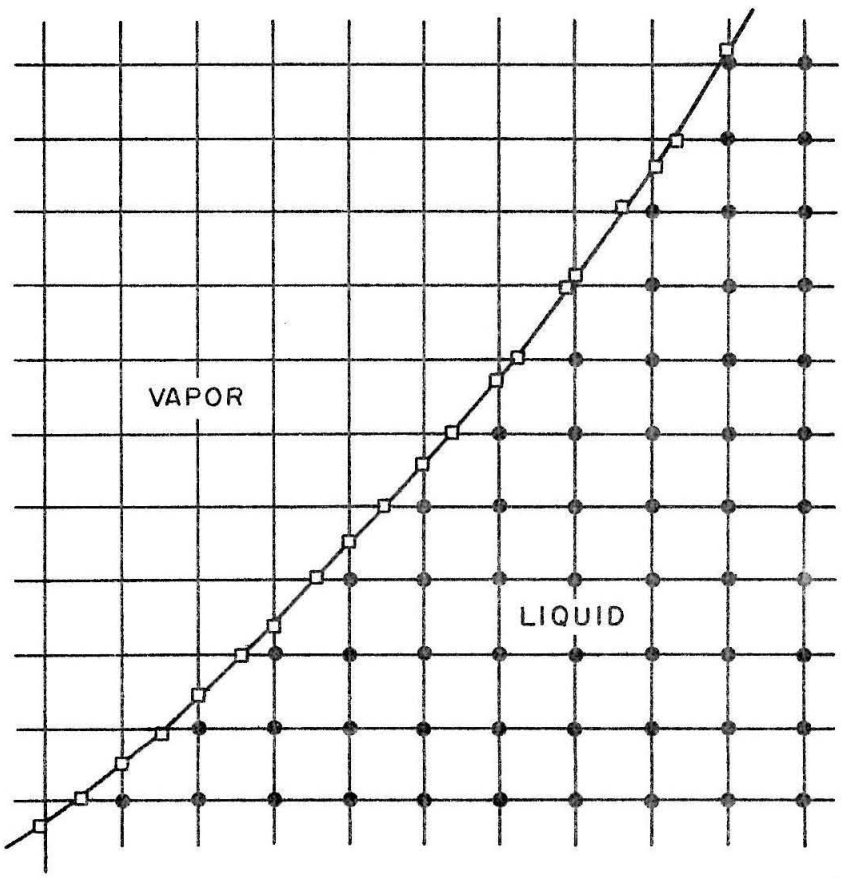

Fig. 2 Representation of the Bubble by Free Boundary Points

Welch, Harlow, Shannon and Daly[11].

The calculations progress by a series of finite time steps or cycles. At the beginning of each cycle the velocity field is known so that the right-hand side of Eq. (I-2) can be evaluated at each cell. Poisson's equation can then be solved by some iterative technique. Once the pressure distribution is known, it can be combined with the known velocities in the equation of motion to find the derivatives of both components of velocity with respect to time. These derivatives are used to establish the velocity at each cell for the next cycle Δt later. The final step in the cycle is to displace the markers, which represent small particles moving with the fluid. In practice there will be several of these markers in each cell. Their velocities are found by simple interpolation. These markers are used to represent streamlines and to define the shape of the free surfaces. The manner in which a cell is treated during a cycle depends on whether it is a full cell containing markers, an empty cell without markers, a free surface cell containing markers but adjacent to an empty cell, or some special case such as a cell adjacent to a solid boundary. After a certain amount of bookkeeping (determining which cells are full, etc.), the next cycle is ready to begin.

Mitchell, Kling, et al raised two main questions in their report. The first question, a common one in flow simulation, is how should the calculations be initiated. They considered bubble collapse caused by an instantaneous decrease of the pressure inside the bubble from the ambient pressure to some fixed lower value. Their concern that this initial pressure discontinuity would somehow persist in the

calculations was not justified; any discontinuity should be smoothed out completely by the initial cycle of the MAC method. The point remains, however, that the initiation of the calculations must be examined closely. It will be seen that an analysis of the early stage of bubble collapse made in Chapter III of this thesis results in improved accuracy and efficiency over this portion of the collapse.

The second question is how can a flow in an unbounded region be described in a necessarily bounded domain. The collapse of a bubble is driven by the difference between the pressure inside the bubble and the pressure infinitely far away. Although interest is centered on the flow near the bubble, the far field cannot be ignored. Rayleigh's solution for the collapse of a spherical bubble stated that the difference between the pressure of the liquid and the ambient pressure is the sum of two terms, which decrease in magnitude like d^{-1} and d^{-4} as d, the distance from the bubble center, is increased. For nonspherical collapse the pressure will have asymmetric terms, which decrease like d^{-2} and faster. One crude method of applying the ambient pressure might be to extend the outer boundary of the domain a number of radii away from the bubble and take the pressure on the outer boundary to be the ambient pressure. A more refined method was provided by Mitchell, Kling, et al, who suggested that Rayleigh's solution for the pressure be used at the outer boundary. The outer boundary should be far enough away from the wall so that the asymmetric terms will have died out. This method is based on the linearized assumption that the spherically symmetric part of the collapse is not affected by the asymmetries of the problem. The

method presented in Chapter III of this thesis avoids this assumption by using an iterative technique for applying the condition at infinity directly to the outer boundary.

Another consideration in applying the MAC method to bubble collapse is one of stability. The theory of Plesset and Mitchell shows that even a small error, or disturbance on the bubble surface, can become significant as the bubble collapses. Any finite difference method will, of course, introduce small errors over the length of a single cell. However, the MAC method is especially crude at free surfaces and can easily give large errors that obscure the results. These errors arise because the MAC method does not modify the finite difference equation at an irregular boundary such as a free boundary but simply imposes the condition that the pressure at the center of a free surface cell is equal to the pressure on the free surface. Modified finite difference equations at an irregular boundary, usually referred to as irregular stars, are essential for an accurate solution near the boundary. In their numerical study of finite-amplitude water waves Chan, Street, and Strelkoff[12] observed that the waveforms became unstable after a few cycles using the MAC method. They obtained satisfactory results, however, with their SUMMAC method, a modified MAC technique using irregular stars at the free surface.

It is apparent that the problem of nonspherical bubble collapse is one which is not readily solved by a general flow simulation method such as the MAC technique. Because nonspherical collapse is of such interest, it is worthwhile to develop a special method from first

principles. This is done most efficiently if the problems of greatest interest are first defined and examined.

II. AN EXAMINATION OF THE PROBLEMS TO BE SOLVED BY NUMERICAL SIMULATION

A. Definition of the Problems of Interest

One problem of interest in nonspherical collapse is to determine the effect of a plane solid wall in deforming a collapsing bubble. Typically a spherical bubble and the liquid surrounding it are visualized as being at rest under a uniform ambient pressure until $t = 0$ when the pressure inside the bubble is instantaneously reduced by Δp. For a compressible liquid this instantaneous pressure drop will produce a shock and an instantaneous radial velocity at the bubble surface[13]

$$\dot{R} = - \frac{\Delta p}{\rho c} \quad , \quad \text{at} \quad t = 0+ \quad . \tag{II-1}$$

An alternate visualization of the problem, entirely equivalent in the incompressible limit, is useful because it eliminates the question of shocks and is more realistic experimentally. The bubble is grown from a small nucleus by the application of a negative ambient pressure. As the bubble grows the ambient pressure is increased continuously to the desired value where it is held constant. The bubble will reach some maximum size and then collapse under the constant ambient pressure. For spherically symmetric growth all segments of the bubble surface will be at rest when the bubble reaches its maximum size. In the incompressible limit the entire liquid will also be at rest. With the absence of shocks compressibility will not become important until speeds in the liquid are comparable with the speed of sound. Thus the liquid can be assumed to be incompressible with the

understanding that solutions are valid for small Mach numbers only.

The asymmetries caused by the solid wall should be separated from those due to initial asymmetries in shape or velocity of the type analyzed by Plesset and Mitchell. The bubble is therefore taken to be initially spherical and at rest, and any other extraneous asymmetric effects such as gravity are also omitted.

The easiest and most widely applicable problem is one which neglects all nonessential features. Therefore the following assumptions will be made.

1. The liquid is incompressible.
2. The flow is nonviscous.
3. The vapor pressure is uniform throughout the bubble interior.
4. The ambient pressure and the vapor pressure are constant with time.
5. The bubble contains no permanent gas.
6. Surface tension effects are negligible.

Only the first three assumptions are essential to the method of simulation developed in this thesis. The last three assumptions are made to keep the essential features of the problem in the foreground. For most cases of bubble collapse the viscous stresses are much smaller than the inertial stresses. Thus in descriptions of bubble collapse, viscosity is usually neglected or kept only as a small refinement. Unlike the spherically symmetric case, which is always irrotational, viscosity must be neglected in nonspherical collapse if strict irrotationality is to be preserved. As for the assumption of

uniform pressure inside the bubble, this assumption will remain valid as long as speeds on the bubble surface are below the speed of sound in the vapor.

The problem is specified by the following conditions:

p_∞ = ambient pressure, (II-2)

p_v = vapor pressure inside the bubble, (II-3)

R_o = initial radius of the bubble, (II-4)

b = initial distance from the plane wall to the center of the bubble. (II-5)

Because the flow is taken to be irrotational, the velocity vector $\vec{v}$ can be written in terms of a velocity potential φ

$$\vec{v}(\vec{x}, t) = \nabla\varphi(\vec{x}, t) \quad . \tag{II-6}$$

The liquid is assumed to be incompressible so that φ must satisfy Laplace's equation throughout the liquid,

$$\nabla^2\varphi(\vec{x}, t) = 0 \quad . \tag{II-7}$$

The pressure boundary conditions, (II-2) and (II-3), can be restated in terms of φ and $v = |\nabla\varphi|$ with the aid of Bernoulli's equation

$$\frac{\partial\varphi}{\partial t} + \frac{v^2}{2} + \frac{p}{\rho} = c(t) \quad . \tag{II-8}$$

Infinitely far from the bubble the velocity is zero, and the pressure is the ambient pressure. The velocity potential is an arbitrary function of time only. Because this function of time has no physical significance it may be taken to be zero,

$$\lim_{|\vec{x}|\to\infty} \varphi(\vec{x}, t) = 0 \quad , \tag{II-9}$$

and since $v \to 0$ at infinity,

$$c(t) = \frac{p_\infty}{\rho} \quad .$$

Then on the free surface,

$$\frac{\partial \varphi}{\partial t} + \frac{v^2}{2} = \frac{p_\infty - p_v}{\rho} = \frac{\Delta p}{\rho} \quad . \tag{II-10}$$

On the solid wall the component of velocity normal to the wall must be zero. Thus

$$\frac{\partial \varphi}{\partial n} = 0 \quad , \quad \text{at the solid wall,} \tag{II-11}$$

where $\frac{\partial}{\partial n}$ denotes the derivative normal to the solid surface. The condition that the liquid is initially at rest may be stated as

$$\varphi(\vec{x}, t) = \text{constant} = 0 \quad \text{when} \quad t = 0 \quad . \tag{II-12}$$

The generality of this problem becomes evident when it is stated in its nondimensional form. Let the nondimensionalized quantities be temporarily denoted by a star. Then the nondimensionalized velocity and displacement are

$$\vec{v}_* = \frac{\vec{v}}{\sqrt{\frac{\Delta p}{\rho}}} \quad \text{and} \quad \vec{x}_* = \frac{\vec{x}}{R_o} \tag{II-13}$$

so that

$$t_* = \frac{t}{R_o}\sqrt{\frac{\Delta p}{\rho}} \quad , \quad \varphi_* = \frac{\varphi}{R_o\sqrt{\frac{\Delta p}{\rho}}} \quad , \text{ etc.}$$

Laplace's equation is unchanged in the nondimensional form as are the homogeneous boundary conditions, (II-9) and (II-11), and the homogeneous initial condition (II-12). The only changes are in the initial conditions, (II-4) and (II-5), and the boundary condition (II-10) which have the nondimensional form:

$$R_{o_*} = \text{initial radius} = 1 \quad , \tag{II-14}$$

$$b_* = \text{initial distance from wall to center of bubble} = \frac{b}{R_o} \quad , \tag{II-15}$$

and

$$\frac{\partial \varphi_*}{\partial t_*} + \frac{v_*^2}{2} = 1 \quad . \tag{II-16}$$

Thus the problem is completely characterized by the single parameter $\frac{b}{R_o}$. The inclusion of surface tension or other effects would have added more parameters and reduced the general applicability of the solution. Now that the nondimensionalized form has been introduced, Eqs. (II-14), (II-15), and (II-16) will be used, but the star notation will be dropped in the sequel.

Another problem of interest is the collapse of a bubble with some asymmetry in its initial shape. A numerical solution is extremely difficult for any three dimensional problem not possessing at least axial symmetry. The shape of any axially symmetric bubble can be described by its radius,

$$r_s(\theta, t) = R(t) + \sum_{n=1}^{\infty} a_n(t) P_n(\cos\theta) \tag{II-17}$$

where P_n is the n'th Legendre polynomial. The odd coefficients

vanish for cases with both plane and axial symmetry. These cases are convenient because the same method developed for collapse near a plane wall may be applied directly to problems with both plane and axial symmetry with the wall forming a plane of symmetry. If it were desired, of course, this method could be easily modified to eliminate the wall.

The same assumptions can apply for this type of problem as for the collapse near a solid wall. The nondimensional forms are also equivalent with the characteristic length being

$$R_o = R(0) = \text{mean radius at } t = 0 \quad .$$

Instead of just a single parameter this problem is characterized by an infinity of parameters:

$$\frac{a_n(0)}{R_o} \quad \text{and} \quad \frac{\dot{a}_n(0)}{\sqrt{\frac{\Delta p}{\rho}}} \qquad n = 2, 4, 6 \ . \ . \ . \ .$$

B. General Characteristics of a Numerical Method Suited to These Problems

Now that the problems of interest have been defined, the general features of a method of flow simulation especially suited to them can be discussed. Clearly the irrotationality of these problems is best exploited by solving them in terms of the velocity potential. A single variable gives a great simplification to almost every aspect of the calculation. If desired, both the velocity and the pressure can be easily calculated from a solution in terms of the potential.

The numerical method should also reflect the fact that the

interest in these problems is centered on the flow at and near the free surface. The shape of the collapsing bubble is of far greater significance than a detailed description of the streamlines far from the bubble. Markers like those used in the Marker-and-Cell method are of little use in representing the results. The task of defining the free surface can be performed by alternate methods so that markers are not needed.

The method used in this thesis calculates the velocity only on the bubble surface. The potential should vary most rapidly near the bubble and vary quite slowly far from the bubble. Thus it is necessary to have a highly accurate and detailed solution near the bubble surface. For a finite difference method this means that the grid should be finest near the free surface. This can be accomplished either by a single nonuniform grid or a series of grids with each successive grid more closely confined to the immediate neighborhood of the bubble and finer than the preceeding grid. The later method is the one used for calculations in this thesis for reasons discussed in Chapter III. The need for an accurate solution in the neighborhood of the free surface also emphasizes the necessity of using irregular stars.

A basic question in the numerical simulation of axially symmetric bubble collapse is whether to base the finite difference scheme on spherical coordinates as was suggested by Mitchell, Kling, et al or on cylindrical coordinates. One advantage of spherical coordinates is that a regular grid in spherical space with the origin inside the bubble will have a greater concentration of points near the bubble than will a regular grid in cylindrical space. The location of the origin of

the spherical system can present a problem, however, especially if the bubble is highly deformed. Because of the singularity, the origin cannot be placed in or adjacent to the liquid. Another disadvantage of spherical coordinates is that the boundary condition at the wall cannot be easily imposed. For a finite difference method based on cylindrical coordinates, the boundary condition at the solid wall is simple and straightforward to apply. For these reasons a finite difference scheme based on cylindrical coordinates was adopted in this thesis. A spherical coordinate system with the origin on the solid wall was used in applying the condition at infinity to the outer boundary, however.

III. DESCRIPTION OF THE NUMERICAL METHOD

A. The Use of Finite Time Steps

All problems considered are axially symmetric so that the bubble and the liquid surrounding it can be described in any half plane bounded by the axis of symmetry. These problems are also assumed to contain a plane solid wall or a plane of symmetry so that they can be further reduced to a single quadrant.

The method of flow simulation is based on a series of finite time steps. The shape and the potential distribution of the free surface forming the bubble is known at the beginning of each time step. The boundary condition at the free surface combined with the condition at infinity and the boundary conditions at the solid wall and the axis of symmetry will determine the potential throughout the liquid. The velocities of points on the free surface can then be calculated. If the time step Δt is small enough, the velocities will remain relatively unchanged throughout the time step. Then the displacement of a point on the free surface with velocity $\vec{v}$ is approximately

$$\Delta\vec{x} = \vec{v}\Delta t \quad . \tag{III-1}$$

Bernoulli's equation is used to get the rate of change of the potential of a point moving with the free surface,

$$\frac{D\varphi}{Dt} = \frac{\partial\varphi}{\partial t} + \vec{v}\cdot\vec{\nabla}\varphi = \frac{\partial\varphi}{\partial t} + v^2 \quad ,$$

in the form

$$\frac{D\varphi}{Dt} = 1 + \frac{v^2}{2} \quad , \tag{III-2}$$

where the nondimensional variables have been used. For Δt small the change in the potential of a displaced point on the free surface is approximately

$$\Delta\varphi = \left(1 + \frac{v^2}{2}\right) \Delta t \quad . \tag{III-3}$$

The velocities in equations (III-1) and (III-3) are, of course, computed at the beginning of the time step. After the free boundary has been displaced and the potentials on it changed accordingly, the new bubble shape with the new potential distribution on the free surface can be used for another time step.

B. The Finite Difference Equations

The finite difference method for solving the potential problem is based on a cylindrical coordinate system (r, z). The r coordinate measures the distance from the axis of symmetry, and the z coordinate measures the distance from the solid wall or the plane of symmetry. Laplace's equation in the case of axial symmetry is

$$\varphi_{rr} + \frac{1}{r}\varphi_r + \varphi_{zz} = 0 \quad . \tag{III-4}$$

Finite difference approximations to Laplace's equation can be found in many places. Shaw[14], in particular, describes the approximation to Eq. (III-4). The domain of interest in the (r, z) plane is covered with a square grid or net formed by a family of horizontal (z = constant) net lines parallel to the solid wall and a family of

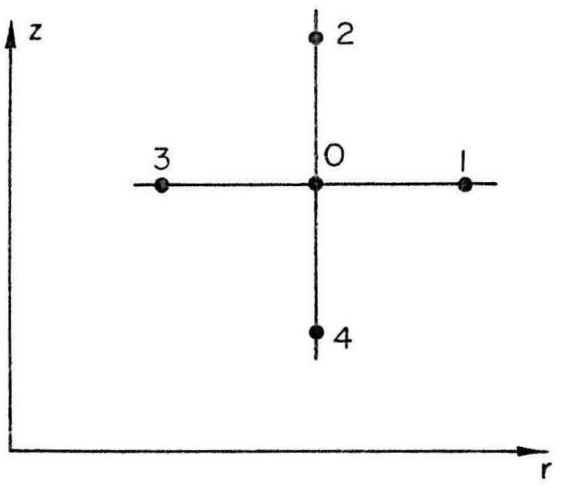

Fig. 3 Numbering System for Stars

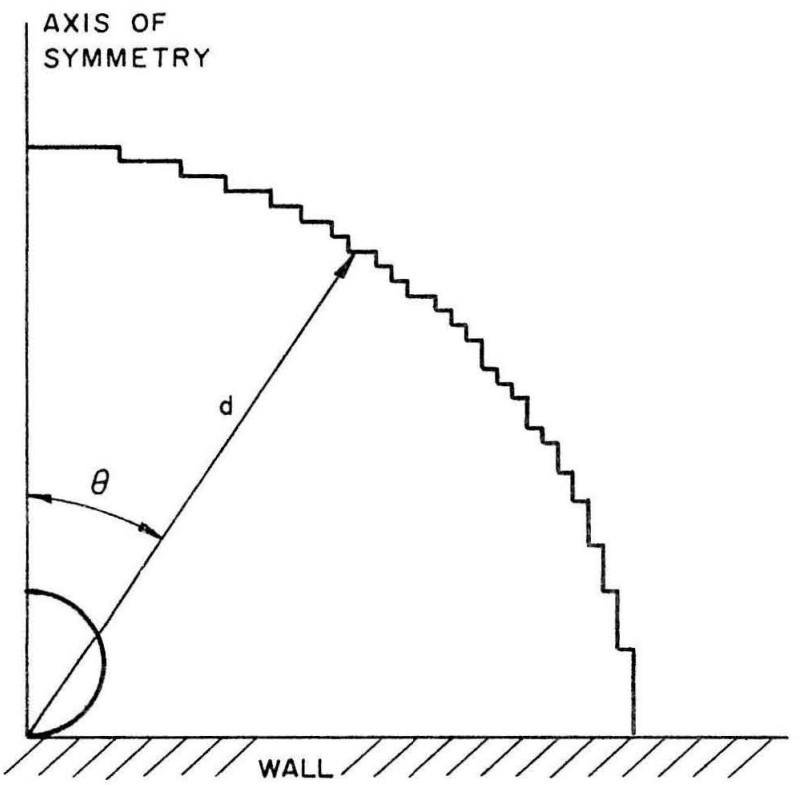

Fig. 4 Net Used to Apply the Condition at Infinity

vertical (r = constant) net lines parallel to the axis of symmetry. Lines of both families are separated by a constant distance h called the mesh length. The potential distribution throughout the liquid is described by the potentials of points, called nodal points, where the two families of net lines intersect. The free boundary is represented in the calculation by the set of points where the free surface and the net lines intersect (see Fig. 2).

A typical nodal point and its four neighboring nodal points, each a distance h from the central point, form a regular star. If a star is centered in the liquid but is near the free surface, some of its outer nodal points may fall inside the bubble. Such stars are called irregular stars because the nodal point inside the bubble must be replaced by a free surface point of known potential creating a leg shorter than the mesh length h. Stars centered inside the bubble are not used in the calculations. The positions of points in both regular and irregular stars with respect to the central or 0 point are identified by the numbering system illustrated in Fig. 3.

The finite difference equation at a star is derived by expanding the potential about the central point and neglecting the higher derivatives (see Shaw, for example). The equation for most regular stars is

$$\varphi_1\left(1 + \frac{h}{2r_o}\right) + \varphi_3\left(1 - \frac{h}{2r_o}\right) + \varphi_4 + \varphi_2 - 4\varphi_o = 0 \qquad \text{(III-5)}$$

where φ_i is the potential at the i'th point of the star and r_o is the distance of the central point from the axis of symmetry. Equation (III-5) may also be written as a formula for the potential of the central

point in terms of the potentials of the other points of the star.

$$\varphi_o = \frac{1}{4}\left[\varphi_4 + \varphi_2 + \varphi_1\left(1 + \frac{h}{2r_o}\right) + \varphi_3\left(1 - \frac{h}{2r_o}\right)\right] \quad . \tag{III-6}$$

Both the boundary conditions on the solid wall and the boundary conditions on the free surface require special treatment for certain stars. Stars centered near the axis of symmetry also need special consideration because of the $\frac{1}{r}\varphi_r$ term in the Laplacian. φ can be expanded for constant z in powers of r about the axis of symmetry,

$$\varphi = a + br^2 + \ldots \qquad (r \text{ small, } z \text{ constant}) \quad . \tag{III-7}$$

A linear term cannot be present in the expansion of φ as a function of r with z fixed since it would imply a line source of fluid on the axis. For a regular star centered on the axis of symmetry

$$\lim_{r \to 0}\left(\varphi_{rr} + \frac{1}{r}\varphi_r\right) = 4b \approx \frac{4(\varphi_1 - \varphi_o)}{h^2} \quad . \tag{III-8}$$

Thus the finite difference approximation is

$$\varphi_2 + \varphi_4 + 4\varphi_1 - 6\varphi_o = 0 \tag{III-9}$$

or

$$\varphi_o = \frac{1}{6}\left[\varphi_2 + \varphi_4 - 4\varphi_1\right] \quad . \tag{III-10}$$

Stars centered directly adjacent to the axis of symmetry at $r = h$ should also be considered. The equation for these stars is also derived from an expansion about the axis of symmetry for constant z. In this case the resulting equation for regular stars is

$$\varphi_o = \frac{1}{2}(\varphi_2 + \varphi_4 + \varphi_1 - \varphi_3) \quad . \tag{III-11}$$

Since the solid wall forms a plane of symmetry, stars centered on the wall must satisfy

$$\varphi_2 = \varphi_4 \quad . \tag{III-12}$$

This condition is imposed simply by using the appropriate star equation with φ_2 substituted for φ_4.

The boundary condition at the free surface enters the calculation through the irregular stars. Equations for these stars contain the sizes of the irregular legs as parameters but are derived in the same way as the corresponding regular star equations. One very minor exception is a star centered at $r = h$ with an irregular point 3 (the point closest to the axis of symmetry). The potential cannot be expanded about the axis in this case because there is no liquid at the axis. The irregular version of Eq. (III-6) is used for this rare case.

C. Solution of the Star Equations Using the Liebmann Method with Overrelaxation.

Each star equation can be written as a formula for the potential of the central point of the star in terms of the central potentials of neighboring stars. The Liebmann iterative method is used with overrelaxation to find the potential distribution that solves all star equations simultaneously. Each iteration of the Liebmann method covers every star in the net column by column. The central potential at each star is, in turn, replaced with a new value based on the star equation. The Liebmann method employs this new potential in the equations of any neighboring stars that are encountered later in the iteration.

This procedure is in contrast with another common method, the Richardson method, which does not use the new potentials until an iteration has been completed. An initial estimate of the potential distribution is necessary to start the Liebmann method. Usually this is provided by the potential distribution from the preceeding time step. The first time steps and time steps immediately following a change in the nets are initiated from a uniformly zero potential.

The convergence of the Liebmann method for large nets is greatly accelerated by the use of overrelaxation[15]. Suppose φ_s is the potential of the central point that satisfies the star equation. Then the old potential φ_{old} is replaced by

$$\varphi_{new} = \varphi_{old} + \alpha(\varphi_s - \varphi_{old})$$

$$1 \leq \alpha < 2 \quad . \tag{III-13}$$

The constant α is called the relaxation factor. A simple estimate of the optimum relaxation factor and the rate of convergence for large nets was developed for the plane case by P.R. Garabedian[16]. He estimated that after N iterations the error would be reduced by a factor of the order of magnitude

$$E = O(e^{-qNh}) \tag{III-14}$$

where q is defined by

$$q = \mathrm{Re}\{2C - \sqrt{4C^2 - 2k_1^2}\} \quad . \tag{III-15}$$

The constant C is related to the relaxation factor by

$$\alpha = \frac{2}{1+Ch} \qquad \text{(III-16)}$$

and k_1 is the lowest eigenvalue of the problem

$$\nabla^2 U + k_n^2 U = 0 \quad . \qquad \text{(III-17)}$$

The boundary conditions on U are the same as on the error in the potential; U is zero on boundaries of known potential and has a zero normal derivative on boundaries where the normal derivative is known.

An analysis analogous to Garabedian's is made of the axially symmetric case in Appendix A. The results are identical if the Laplacian in Eq. (III-17) is taken in its three dimensional form. Clearly convergence is most rapid when q is maximized. Garabedian pointed out that if C is made greater than $k_1/\sqrt{2}$, the real part of $-\sqrt{4C^2 - 2k_1^2}$ will decrease sharply reducing convergence considerably, but if C is less than or equal to the optimum $k_1/\sqrt{2}$, then $-\sqrt{4C^2 - 2k_1^2}$ is purely imaginary so that

$$q = 2\,\frac{(2-\alpha)}{\alpha h} \quad . \qquad \text{(III-18)}$$

If we assume that α is large enough to cover the lowest eigenvalue, i.e.

$$\alpha \geq \frac{2}{\dfrac{kh}{1 + \dfrac{1}{\sqrt{2}}}} = \alpha_{\text{optimum}} \quad , \qquad \text{(III-19)}$$

then the rate of convergence is a function of α only,

$$E = O\left(\exp -N\left(\frac{4-2\alpha}{\alpha}\right)\right) \quad . \qquad \text{(III-20)}$$

A useful example is that of two concentric spheres with known

potential distributions on their surfaces. Let d measure the distance from their common center. If the radii of the inner sphere and the outer sphere are d_i and d_o respectively, the boundary condition on U is

$$U = 0 \quad , \quad \text{at } d = d_i \quad \text{and} \quad d = d_o \quad . \tag{III-21}$$

The eigenfunction with the smallest eigenvalue is a linear combination of the zeroth order spherical Bessel functions, $j_o(k, r)$ and $y_o(k, r)$. From the boundary conditions

$$U_1 = \frac{\sin k_1(d-d_i)}{d} \tag{III-22}$$

where

$$k_1 = \frac{\pi}{d_o - d_i} = \frac{\pi}{Jh} \tag{III-23}$$

is the smallest eigenvalue and J is the number of mesh lengths between spheres. The optimum relaxation factor is then

$$\alpha_{\text{optimum}} = \frac{2}{1 + \frac{\pi}{\sqrt{2J}}} \quad . \tag{III-24}$$

If the relaxation factor is this optimum value, then the error reduction factor is

$$E = O\left(\exp - N\left(\frac{\sqrt{2}\,\pi}{J}\right)\right) \quad . \tag{III-25}$$

The number of iterations necessary to achieve a given error reduction is proportional to J.

The finite difference approximation to Laplace's equation, the

Liebmann method, and overrelaxation are all well-known techniques that have been applied to many different problems. The more specialized aspects of the method associated with the present problem will now be discussed.

D. The Condition at Infinity Applied to the Outer Boundary

It was stated in Chapter I that an iterative method has been developed for applying the condition at infinity to the outer boundary. The outer boundary in this case refers to the boundary of the net excluding the free boundary, the axis of symmetry, and the solid wall. The method is based on a spherical coordinate system (d, θ) with its origin at the intersection of the axis of symmetry and the solid wall. The distance from the origin is d; the angle with the axis of symmetry is θ. Each step begins with a net like the one in Fig. 4. The shape of this net is chosen to give the nodal points on the outer boundary a nearly constant value of d. A slight point to point variation in d is unimportant, however. Irregular stars are unnecessary on the outer boundary. The average value of d on the outer boundary will be referred to as d_o.

The potential can be expanded in a series of axially symmetric harmonics that will be valid for values of d large enough to completely contain the bubble

$$\varphi(d,\theta) = \sum_{k=o}^{\infty} (A_{2k} d^{2k} + B_{2k} d^{-(2k+1)}) P_{2k}(\cos\theta) \quad . \qquad \text{(III-26)}$$

Only the even Legendre polynomials are used in the expansion because of the symmetry of the plane wall. The condition that the potential

approaches zero infinitely far from the bubble may be restated as

$$A_{2n} = 0 \qquad n = 1,2,3 \ldots \qquad \text{(III-27)}$$

The A coefficients will be zero only when the potential distribution on the outer boundary is consistent with the condition at infinity.

The higher harmonics should die out most rapidly as d increases. It is assumed that d_o is large enough so that the $P_o(\cos\theta)$ and $P_2(\cos\theta)$ terms effectively describe the potential on the outer boundary. The $P_4(\cos\theta)$ term is also included in the calculation, but d_o is large enough in practice to keep this term negligible. The potential at the outer boundary may then be written as

$$\varphi(d_o,\theta) = \left(A_o + \frac{B_o}{d_o}\right) + \left(A_2 d_o^2 + \frac{B_2}{d_o^3}\right) P_2(\cos\theta) + \left(A_4 d_o^4 + \frac{B_4}{d_o^5}\right) P_4(\cos\theta)$$

$$= C_o + C_2 P_2(\cos\theta) + C_4 P_4(\cos\theta) \quad . \qquad \text{(III-28)}$$

Each time step begins with a trial potential distribution on the outer boundary. This potential distribution is usually provided by the results of the previous time step. The potential problem is solved using these trial outer boundary values for the potential. The condition that the A coefficients must vanish may be stated as a relationship between the potential and its radial derivative. Therefore, the radial derivative is calculated at each nodal point on the outer boundary. All nodal points on the outer boundary of nets like the one in Fig. 4 have other nodal points directly below them and to their left. The derivative in the vertical direction can be calculated by fitting a second order polynomial through the outer boundary nodal point (r,z) and the two

nodal points directly below it. From Eq. (III-46), which is derived in Section F of this chapter, one obtains

$$h \frac{\partial \varphi}{\partial z} (r,z) \approx 2(\varphi(r,z) - \varphi(r,z-h)) - \frac{1}{2}(\varphi(r,z) - \varphi(r,z-2h)) \quad . \text{(III-29)}$$

The horizontal derivative is calculated by the same method and is then combined with the vertical derivative to produce the radial derivative:

$$\begin{aligned} \frac{\partial \varphi}{\partial d} (d_o, \theta) &= \left|\frac{\partial \varphi}{\partial z}\right|_r \cos\theta + \left|\frac{\partial \varphi}{\partial r}\right|_z \sin\theta \\ &= -\frac{B_o}{d_o^2} + \left(2A_2 d_o - 3\frac{B_2}{d_o^4}\right) P_2(\cos\theta) \\ &\quad + \left(4A_4 d_o^3 - 5\frac{B_4}{d_o^6}\right) P_4(\cos\theta) \\ &\equiv D_o + D_2 P_2(\cos\theta) + D_4 P_4(\cos\theta) \quad . \end{aligned} \text{(III-30)}$$

The C and D coefficients are easily evaluated from the potential on the outer boundary and its radial derivative. The A and B coefficients are determined by the C and D coefficients. In particular,

$$\begin{aligned} B_o &= -D_o d_o^2 \\ B_2 &= (2C_2 d_o^3 - D_2 d_o^4)/5 \quad , \\ \text{and} \qquad B_4 &= (4C_4 d_o^5 - D_4 d_o^6)/9 \quad . \end{aligned} \text{(III-31)}$$

The condition that the A coefficients vanish can be stated as a relationship between the C and B coefficients or, equivalently, between the C and D coefficients:

$$C_o = B_o/d_o = - D_o d_o \quad ;$$

$$C_2 = B_2/d_o^3 = (2C_2 - D_2 d_o)/5 \quad ;$$

$$C_4 = B_4/d_o^5 = (4C_4 - D_4 d_o)/9 \quad . \qquad \text{(III-32)}$$

With the neglect of the higher harmonics, Eqs. (III-32) will be satisfied only when the potentials on the outer boundary are consistent with the condition at infinity. Equations (III-32) suggest that the B coefficients calculated from Eqs. (III-31) may be used to form new potentials at the outer boundary nodal points from the formula

$$\varphi(d,\theta) = \frac{B_o}{d} + \frac{B_2}{d^3} P_2(\cos\theta) + \frac{B_4}{d^5} P_4(\cos\theta) \quad . \qquad \text{(III-33)}$$

The iteration scheme is to solve the potential problem with the new outer boundary potentials, then find the B coefficients from Eqs. (III-31) and use them in Eq. (III-33) to establish outer boundary potentials for the next iteration. Let a superscript n on a coefficient denote the value of that coefficient during the n'th iteration. Equation (III-33) specifies that

$$C_o^{n+1} = B_o^n/d_o = - D_o^n d_o \quad ,$$

$$C_2^{n+1} = B_2^n/d_o^3 = (2C_2^n - D_2^n d_o)/5 \quad ,$$

$$C_4^{n+1} = B_4^n/d_o^5 = (4C_4^n - D_4^n d_o)/9 \quad . \qquad \text{(III-34)}$$

If the coefficients converge, they will converge to a solution of Eqs. (III-32).

The convergence of this method can be studied analytically for

the simple case of a perfectly hemispherical bubble on a solid wall with an axially symmetric potential distribution on the bubble surface. Let d_i be the radius of the bubble. The potential on the bubble surface may be expanded as

$$\varphi(d_i, \theta) = \sum_{k=o}^{\infty} F_{2k} P_{2k}(\cos\theta) \quad . \tag{III-35}$$

Then the correct potential at the outer boundary is

$$\varphi(d_o, \theta) = F_o\left(\frac{d_i}{d_o}\right) + F_2\left(\frac{d_i}{d_o}\right)^3 P_2(\cos\theta) + F_4\left(\frac{d_i}{d_o}\right)^5 P_4(\cos\theta) + \ldots \tag{III-36}$$

The ratio $\frac{d_i}{d_o}$ is assumed to be sufficiently small so that higher harmonics are negligible at the outer boundary. Let the error in the potential at the outer boundary be expanded in Legendre polynomials:

$$\varphi^n(d_o, \theta) - \varphi(d_o, \theta) = E_o^n + E_2^n P_2(\cos\theta) + E_4^n P_4(\cos\theta) + \ldots \tag{III-37}$$

Then from Eq. (III-36) the coefficients are given by

$$\begin{aligned}
E_o^n &= C_o^n - F_o\left(\frac{d_i}{d_o}\right) = A_o^n + \frac{B_o^n}{d_o} - F_o\left(\frac{d_i}{d_o}\right) \quad , \\
E_2^n &= C_2^n - F_2\left(\frac{d_i}{d_o}\right)^3 = A_2^n d_o^2 + \frac{B_2^n}{d_o^3} - F_2\left(\frac{d_i}{d_o}\right)^3 \quad , \\
E_4^n &= C_4^n - F_4\left(\frac{d_i}{d_o}\right)^5 = A_4^n d_o^4 + \frac{B_4^n}{d_o^5} - F_4\left(\frac{d_i}{d_o}\right)^5 \quad .
\end{aligned} \tag{III-38}$$

Since the potential is known on the free surface the solution there is always correct. Thus

$$A_o^n + B_o^n/d_i = F_o \quad ,$$

$$A_2^n d_i^2 + B_2^n/d_i^3 = F_2 \quad , \qquad \text{(III-39)}$$

and $$A_4^n d_i^4 + B_4^n/d_i^5 = F_4 \quad .$$

Equations (III-38) can be combined with Eqs. (III-39) to obtain

$$B_o^n = F_o d_i + E_o^n \frac{d_o d_i}{d_o - d_i} \quad ,$$

$$B_2^n = F_2 d_i^3 + E_2^n \frac{d_o^3 d_i^3}{d_o^3 - d_i^3} \quad , \qquad \text{(III-40)}$$

and

$$B_4^n = F_4 d_i^5 + E_4^n \frac{d_o^5 d_i^5}{d_o^5 - d_i^5}$$

From Eqs. (III-34) the C and E coefficients for the next iteration will be

$$C_o^{n+1} = F_o\left(\frac{d_i}{d_o}\right) + E_o^n \frac{d_i}{d_o - d_i} \quad , \quad \left(E_o^{n+1} = E_o^n \frac{d_i}{d_o - d_i} \right) \quad ,$$

$$C_2^{n+1} = F_2\left(\frac{d_i}{d_o}\right)^3 + E_2^n \frac{d_i^3}{d_o^3 - d_i^3} \quad , \left(E_2^{n+1} = E_2^n \frac{d_i^3}{d_o^3 - d_i^3} \right) \quad , \qquad \text{(III-41)}$$

and

$$C_4^{n+1} = F_4\left(\frac{d_i}{d_o}\right)^5 + E_4^n \frac{d_i^5}{d_o^5 - d_i^5} \quad , \left(E_4^{n+1} = E_4^n \frac{d_i^5}{d_o^5 - d_i^5} \right) \quad .$$

If d_i/d_o is small, then the errors can be greatly reduced in

a single iteration. It is now obvious why more terms were not included in the calculation to improve the validity for smaller values of d_o; convergence is enhanced by keeping the radius of the outer boundary large. In practice three or four iterations were sufficient to establish a satisfactory potential distribution on the outer boundary starting from a uniformly zero distribution, and only a single iteration was necessary to adjust for the small changes between consecutive time steps.

The net used to establish the outer boundary potentials had a radius of 40 mesh lengths or, occasionally, 50 mesh lengths. The initial bubble shape had a radius of 5 mesh lengths in this net for the problem of an initially spherical bubble collapsing near a solid wall and a mean radius of 10 mesh lengths for the problem of an initially nonspherical bubble collapsing in a homogeneous liquid.

One case, for example, started with a nonspherical bubble with a radius of

$$d_i = 1 - \frac{1}{10} P_2(\cos\theta) \qquad \text{(III-42)}$$

where

$$\text{mean radius} = 1 = 10 \text{ mesh lengths} \quad .$$

The radius of the outer boundary was four times the mean radius of the bubble. The potential was unity over the entire bubble surface. Since the deviation from spherical (or hemispherical) was only ten percent, a first order estimate of C_o and C_2 can be made by linearizing the condition on the free surface. To first order

$$1 \approx \frac{B_o}{d_i} + \frac{B_2}{d_i^3} P_2(\cos\theta) + \ldots$$

$$\approx B_o\left[1 + \frac{1}{10} P_2(\cos\theta)\right] + B_2 P_2(\cos\theta) + \ldots \qquad \text{(III-43)}$$

so that

$$B_o \approx 1.0 \quad \text{or} \quad C_o \approx 0.25$$

and

$$B_2 \approx -0.1 \quad \text{or} \quad C_2 \approx -0.0016 \quad .$$

This gives a rough check on the values actually computed, which are listed in Table I. Differences are due to second order terms neglected in Eq. (III-43) and the fact that the accuracy of the numerical solution is limited because the free surface is represented by only a finite number of points in this net, twenty-one in this case.

TABLE I

Values of the C Coefficients Computed while Establishing a Potential Distribution on the Outer Boundary

Iteration	C_o^n	C_2^n	C_4^n
initial values	0.0	0.0	0.0
n = 1	0.28664	-0.0042862	0.0018235
n = 2	0.24474	-0.00010602	-0.00057663
n = 3	0.25159	-0.0014508	0.000044342
n = 4	0.25038	-0.0013336	-0.000018905
n = 5	0.25060	-0.0013661	-0.0000094077

An examination of Table I shows that the convergence of the coefficients does not follow Eqs. (III-41). The C_o^n coefficient converges

more rapidly than expected; while C_2^n, which should converge faster than C_o^n, does not converge at all until C_o^n is somewhat settled. Finally C_4^n, which should converge the fastest of all, merely declines in magnitude without approaching a limiting value. One possible explanation is that the asymmetry of the bubble shape has coupled the coefficients. If d_i is no longer a constant, then Eqs. (III-39) will be coupled causing the coefficients of the error to couple. But this coupling cannot explain, for example, why C_2^n and C_4^n are erratic during the first few iterations while C_o^n converges. The true cause is revealed by the observation that an increase in the number of iterations used by the Liebmann method reduces this type of behavior. Any change in C_o^n or any other of the coefficients alters the outer boundary potentials and introduces an error in the potential solution near the outer boundary. The Liebmann method reduces this error by a factor depending on the number of iterations used. The overall effect of the reduced error should be much smaller than the change in the potentials. But if the changes in the outer boundary potentials are much larger than C_2 or C_4, the reduced error may still have a large effect on them. In this case C_2 is much smaller than C_o, and C_4 is negligible. Thus C_2^n and C_4^n are highly susceptible to changes in C_o^n as has been observed. This does not pose a practical problem, however, since it is of no value to determine C_2 and C_4 more accurately than C_o.

The accuracy of the coefficients is enhanced by keeping the number of points used to represent the free surface as large as possible. Convergence demands that the outer boundary of the net be as far as possible from the bubble. Both these conditions can best be

simultaneously satisfied for cases in which the bubble is close to the solid wall. Then as the bubble collapses, the scale of the net used to establish the outer boundary potentials can be halved from time to time. This procedure effectively moves the outer boundary closer to the free surface. The outer potentials are then re-established. In practice these potentials were observed to be consistent with their values during the preceeding time step when the new outer boundary points were interior points. Values of the C coefficients for time steps immediately before and after a typical scale change are presented in Table II.

TABLE II

Values of the C Coefficients for Time Steps Immediately Before and After a Typical Scale Change

	C_o	C_2	C_4
time step preceeding scale change	0.1377	0.0002603	0.0000754
time step following scale change	0.2699	0.002600	-0.0000292

Ideally, neglecting the change between consecutive time steps, C_o should be doubled and C_2 increased by a factor of eight. The second set of coefficients is the more accurate since the net used to find them contained twenty-four free boundary points while the net used for the first set contained only twelve free surface points.

E. The Application of a Series of Nets to Obtain a Detailed Solution

Once the potentials on the outer boundary are established, they are applied in the solution of the potential problem. The large mesh

length of the net used to establish the outer boundary potentials gives only a rough solution near the free boundary. Therefore a series of progressively finer nets is used to provide a more detailed description there. Another possibility would be to use a large single net composed of various regions of uniform mesh length with the mesh lengths of these regions decreasing as the free surface is approached. This would have one advantage in that a more detailed description of the free surface would increase the accuracy of the outer boundary potentials. If this single net contained a large number of points, however, the convergence of the Liebmann method could be quite slow. It can be seen from Garabedian's results that the number of Liebmann iterations needed for a given factor of error reduction is, assuming a uniform mesh, inversely proportional to the mesh length. Thus the total number of operations required is inversely proportional to the cube of the mesh length. If a detailed solution of a potential problem is required, it is more economical to first obtain a solution using a coarse net and then apply the finer nets[17]. Thus a series of nets is the most efficient method for obtaining a detailed solution near the free boundary.

It is convenient if each net of the series has a mesh length half the mesh length of the preceeding net. Then a nodal point of the finer net falls either directly on the location of a nodal point in the preceeding net, midway between two such points, or equidistant from four of these points. In the first case the initial potential is taken directly from the preceeding net. The potentials must be averaged in the other two cases. Since each net of the series is contained in the preceeding one, the outer boundary potentials are taken from the preceeding net.

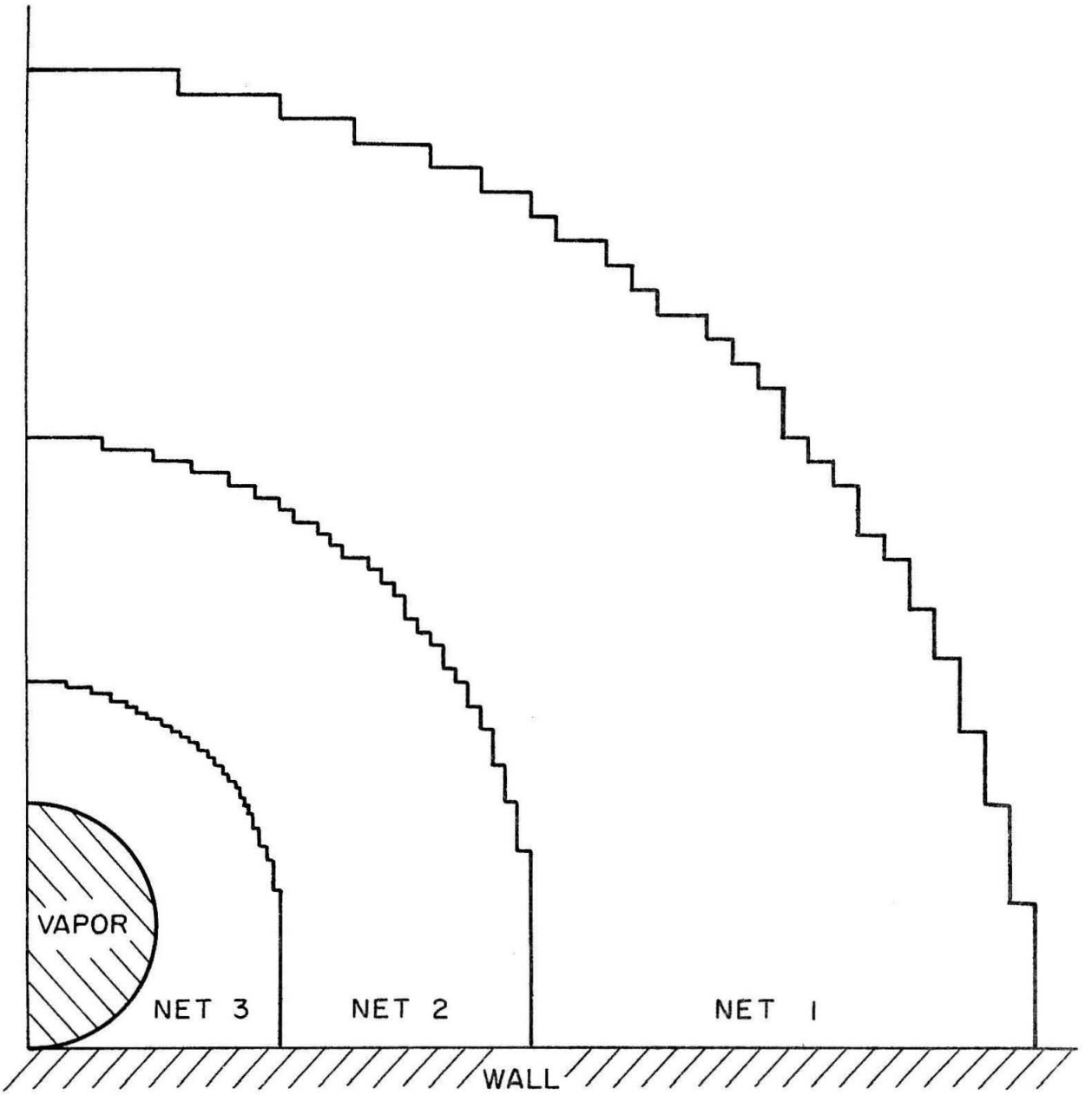

Fig. 5 A Typical Series of Nets
(Each Net Extends to the Bubble Surface)

The shapes of all nets except the first one of the series are arbitrary. Usually these nets were shaped to give a minimum distance of ten to twenty mesh lengths between the free surface and the outer boundary. A typical series of nets is illustrated in Fig. 5.

In practice either three or four nets were used in the series. The finer nets had a large percentage of their nodal points located in the bubble interior. Although these "interior" points have no active role in the calculations, they do occupy storage. Since the number of these points quadruples when the mesh length is halved, storage requirements can limit the number of nets that can be used in a series. For an initially spherical bubble collapsing near a solid wall the final net contained an average of 100 free surface points. Because of the plane of symmetry, the final net contained an average of 50 free surface points for the case of a nonspherical bubble with axial and plane symmetry collapsing in a homogeneous liquid. Whenever the number of free boundary points fell below these levels, another net was added to the series. Whenever the scale of the first net was halved, a net was subtracted from the series.

The relaxation factor for the first net of the series was estimated from the model of a sphere of radius d_o with a point of known potential (representing the free boundary) at its center. The optimum relaxation factor for $J = 40$ is $\alpha = 1.895$ from Eq. (III-24). After N Liebmann iterations, the error will then be reduced by a factor of $E = O(\exp(0.111N))$. Thus 40 iterations will reduce the error by a factor of about 85. This is enough to adjust for the small changes between consecutive time steps. The changes in the outer boundary

potentials between consecutive time steps are always much smaller than the changes at the free boundary. The potential problem is solved at least twice using the first net of each time step, once to establish the new outer potentials and once using them. Thus the first net is subject to at least 80 iterations under the proper free boundary conditions. If the outer potentials must be established from a uniformly zero distribution, an increased number of iterations such as 50 is advisable because of the large changes at the outer boundary.

The finer nets contain errors of predominantly small wavelengths. For these nets a relaxation factor capable of handling errors extending a distance of 20 meshlengths from a spherical boundary should be adequate. From Eq. (III-24) $\alpha = 1.80$ when $J = 20$. The initial errors in the finer nets will be small in magnitude. Also errors near the free boundary left by one net will be reduced by following nets. Therefore 15 iterations should be sufficient for the intermediate nets. This gives an error reduction factor of about 30 for $\alpha = 1.80$. Although the initial errors are quite small, more iterations are advisable for the final net of the series because the velocities at the free surface points are calculated from its solution. A choice of 25 iterations gives an error reduction factor of about 250 for $\alpha = 1.80$.

The potentials of typical points near the free surface as they appear in the various nets of the series give some insight into the calculations. Two examples are given here. In the example presented in Table III, the points are on a horizontal net line and three nets are used in the series. In the example presented in Table IV, the points are on a vertical net line (as in Fig. 6) and four nets form the series.

The symbol h_i refers to the mesh length of the i'th net of the series.

TABLE III

Example of Potentials Near the Free Surface on a Horizontal Net Line

distance along net line from free surface	potential in first net	potential in second net	potential in third net
0	0.4376928	0.4376928	0.4376928
$0.8421\,h_3$			0.4237445
$1.8431\,h_3$	0.4078838	0.4085018	0.4084863
$2.8421\,h_3$			0.3944585
$3.8421\,h_3$		0.3815605	0.3815108
$4.8421\,h_3$			0.3695085
$5.8421\,h_3$	0.3577823	0.3584075	0.3583410

TABLE IV

Example of Potentials Near the Free Surface on a Vertical Net Line

distance along net line from free surface	potential in first net	potential in second net	potential in third net	potential in fourth net
0	1.77944	1.177944	1.77944	1.177944
$0.5917\,h_4$				1.150050
$1.5917\,h_4$			1.105793	1.105800
$2.5917\,h_4$				1.064858
$3.5917\,h_4$		1.027130	1.027021	1.026908
$4.5917\,h_4$				0.991664
$5.5917\,h_4$			0.959042	0.958863
$6.5917\,h_4$				0.928276
$7.5917\,h_4$	0.897183	0.900305	0.899897	0.899693

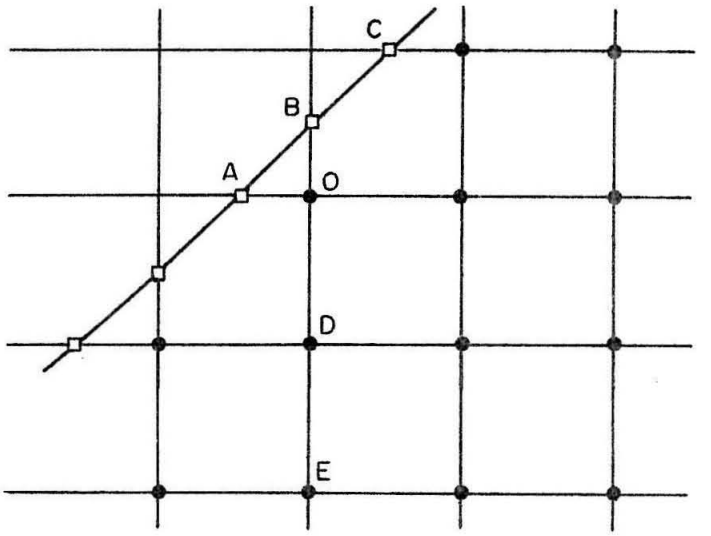

Fig. 6 Points Used to Calculate the Velocity at Free Boundary - - Point B

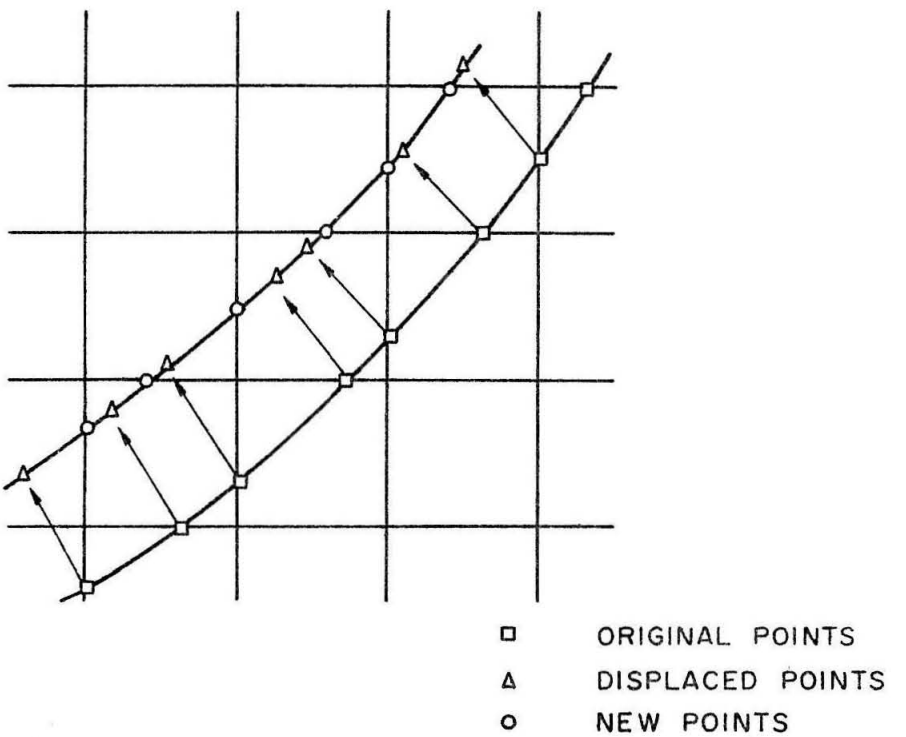

Fig. 7 Linear Interpolation to Obtain New Boundary Points

These examples show that the potential at a point changes only slightly between consecutive nets of the series; the errors in the initial potentials of the finer nets are small, as expected. They also show that the potential in the final net varies smoothly with the distance from the free boundary and can be described accurately by a quadratic over the distance of a few mesh lengths. This behavior is useful in the velocity calculations.

F. Calculation of Velocities on the Free Surface

The velocity components in both the r and z directions must be found at all free boundary points of the final net. Each free boundary point will lie on either a vertical net line or a horizontal net line. The velocity calculation will be described for a point on a vertical net line. The method is completely analogous for points on horizontal net lines. If the mesh length of the final net is sufficiently small, each free boundary point will be part of an irregular star with a regular point opposite the free boundary point as in Fig. 6. The only exception for free boundary points on vertical net lines occurs when the bubble touches the wall with an acute angle of contact. Then there are stars with irregular vertical legs centered on the solid wall. Let φ_B, φ_o, and φ_D be the potentials of the free boundary point, the central point of the irregular star, and the point opposite the free boundary point, respectively. The potential along the vertical net line is approximated near the free boundary point by a quadratic fitted through points B, O, and D. Writing this quadratic as an expansion about the boundary point for a constant r gives the form

$$\varphi = \varphi_B + a(z-z_B) + b(z-z_B)^2 \quad . \qquad \text{(III-44)}$$

The coefficients a and b are determined from the potentials at points O and D. The vertical velocity is then

$$\left(\frac{\partial\varphi}{\partial z}\right)_B = a = (z_D-z_o)^{-1}\left[\left(\frac{z_D-z_B}{z_o-z_B}\right)(\varphi_o-\varphi_B) - \left(\frac{z_o-z_B}{z_D-z_B}\right)(\varphi_D-\varphi_B)\right] \quad . \qquad \text{(III-45)}$$

Or, since $|z_D-z_o| = h$,

$$\left(\frac{\partial\varphi}{\partial z}\right)_B = \frac{\operatorname{sgn}(z_D-z_B)}{h}\left[\frac{\lambda+1}{\lambda}(\varphi_o-\varphi_B) - \frac{\lambda}{\lambda+1}(\varphi_D-\varphi_B)\right] \qquad \text{(III-46)}$$

where

$$\lambda = \frac{z_o-z_B}{z_D-z_o} = \frac{|z_o-z_B|}{h} = \frac{\text{length of irregular leg}}{\text{length of regular leg}} \quad .$$

When λ is smaller than some minimum value λ_{Min}, point D is used in place of point O, and the next point along the net line (point E in Fig. 6) replaces point D. This adds unity to λ.

If the irregular star is centered on the solid wall, the potential may be expanded about the wall along a vertical net line. Since the potential is an even function of z,

$$\varphi = \varphi_o + bz^2 + \ldots \quad \text{(for } \mathbf{r} = \text{constant)} . \qquad \text{(III-47)}$$

Thus the vertical velocity may be approximated by

$$\frac{\partial\varphi}{\partial z} \approx 2b\,z_B \approx \frac{2(\varphi_B-\varphi_o)}{z_B} \quad . \qquad \text{(III-48)}$$

Once the derivative in the vertical direction has been found, the derivative in the horizontal direction can be calculated from the two

free boundary points on either side of point B, points A and C. A linear approximation is used for the potential between adjacent free surface points. Expansion of the potential about point B along the free surface gives to first order the form

$$\varphi_A \approx \varphi_B + \left(\frac{\partial\varphi}{\partial z}\right)_B (z_A - z_B) + \left(\frac{\partial\varphi}{\partial r}\right)_B (r_A - r_B) \quad . \tag{III-49}$$

Equation (III-49) produces an estimate for the horizontal velocity,

$$\left(\frac{\partial\varphi}{\partial r}\right)_B \approx \frac{\varphi_A - \varphi_B - \left(\frac{\partial\varphi}{\partial z}\right)_B (z_A - z_B)}{(r_A - r_B)} \quad . \tag{III-50}$$

To avoid any systematic errors, this estimate is averaged with another estimate of $\left(\frac{\partial\varphi}{\partial r}\right)_B$ made using the free surface point C on the other side of B. Since the method for finding the horizontal velocity is essentially to subtract the known vertical component from the velocity tangential to the free surface, the tangent to the free surface cannot be nearly vertical if accurate results are desired. If the normal to the free surface makes too small an angle with the horizontal direction, then the velocities are not calculated at that point, and the point will not be used in forming the displaced free boundary for the next time step. Similarly free boundary points on horizontal net lines are not used where the normal to the free surface is nearly vertical. The percentage of points eliminated by this criterion is small, however, since the free surface will cross few vertical net lines where its normal is nearly horizontal and vice versa. It is also wise to eliminate one of a pair of adjacent free surface points that are extremely close to each other (a few hundredths of a mesh length) since there is a

chance that their paths may cross when they are displaced.

After the free boundary points of the final net are displaced according to Eq. (III-1) and have had their potentials changed according to Eq. (III-3), they are used with the proper scaling to define the free boundary in all of the nets of the next time step. These displaced points are not directly applicable, however, since they do not in general fall on the net lines. To obtain the points where the free surface intersects the net lines, consecutive pairs of displaced points are connected by straight lines as illustrated in Fig. 7. A free boundary point is established wherever one of these lines intersects a net line. Its potential is determined by linear interpolation between the endpoints.

G. Special Treatment for the Initial Time Step and the Early Stage of Collapse

Equations (III-1) and (III-3) are accurate only if the velocities are relatively constant between consecutive time steps. The criterion to be used in choosing the size of a time step should be that the velocities of the free boundary points must change by less than a given percentage between consecutive time steps. This is clearly impossible for the first time step if the velocities are initially zero. By examining the early stage of the collapse, however, Eqs. (III-1) and (III-3) can be modified to give greater efficiency and accuracy for the beginning time steps.

Consider a bubble completely at rest at t=0. Early in the collapse all velocities will be small. At a point on the free surface

$$\left|\frac{D\vec{x}}{Dt}\right| = v \ll 1 \quad , \tag{III-51}$$

and

$$\frac{D\varphi}{Dt} = 1 + \frac{1}{2} v^2 = 1 + O(v^2) \quad . \tag{III-52}$$

As a first approximation take the velocity to be zero in Eqs. (III-51) and (III-52). Then the initial shape of the bubble will remain unchanged, and the potential will have a uniform value of

$$\varphi = t \qquad \text{over the free surface.} \tag{III-53}$$

The potential distribution throughout the liquid is then

$$\varphi(\vec{x}, t) = G(\vec{x})t \tag{III-54}$$

where $G(\vec{x})$ satisfies

$$\nabla^2 G(\vec{x}) = 0 \quad \text{throughout the liquid,} \tag{III-55}$$

$$G(\vec{x}) \to 0 \quad \text{as} \quad |\vec{x}| \to \infty \quad , \tag{III-56}$$

$$G(\vec{x}) = 1 \quad \text{on the initial free surface} \quad . \tag{III-57}$$

Now the gradient of the potential is

$$\nabla\varphi(\vec{x}, t) = \vec{V}(\vec{x}) \cdot t \tag{III-58}$$

where

$$\vec{V}(\vec{x}) = \nabla G(\vec{x}) \quad . \tag{III-59}$$

As a second approximation take

$$\vec{v}(\vec{x}, t) = t \cdot \vec{V}(\vec{x}) \quad . \tag{III-60}$$

Then after an initial time step of Δt_1 ,

$$\Delta\vec{x} = \vec{V}(\vec{x}) \int_0^{\Delta t_1} t\,dt = \frac{1}{2}\,\vec{V}(\vec{x})(\Delta t_1)^2 \qquad \text{(III-61)}$$

and

$$\varphi(\vec{x}) = \int_0^{\Delta t_1} \left[1 + \frac{1}{2}\,V^2(\vec{x})t^2 \right] dt = \Delta t_1 \left[1 + \frac{1}{6}\,V^2(\vec{x})(\Delta t_1)^2 \right] . \qquad \text{(III-62)}$$

For the initial time step the potential problem is set up with the initial free surface at a potential of unity. The resulting velocities at free surface points are used in Eqs. (III-61) and (III-62) to find the displacements and potentials of these points.

Since the radius or the mean radius is initially unity in the non-dimensional form, the magnitude of $\vec{V}(\vec{x})$ is of order unity. Thus Eqs. (III-61) and (III-62) improve Eqs. (III-1) and (III-3) by adding terms of order $(\Delta t_1)^2$. Further refinements would add terms of order $(\Delta t_1)^4$ and higher. The method used for the two cases discussed in Chapter IV was to take an initial time step based on Eqs. (III-61) and (III-62) followed by time steps based on Eqs. (III-1) and (III-3). The changes in velocities between consecutive time steps immediately following the initial time step must be small compared to the velocities established by the initial time step. Therefore the initial time step was made as large as possible $(\Delta t_1 = 0.25)$ subject to the condition that $(\Delta t_1)^4 \ll 1$.

An improved method was used for the two cases discussed in Chapter V. Equations (III-1) and (III-3) are correct if the velocities of the free surface points remain constant while they are displaced. An estimate of the behavior of the velocity during the initial time step led to Eqs. (III-61) and (III-62). The rate of change of the velocity can be

similarly estimated for all time steps in the early stage of collapse. This portion of the collapse is characterized by low velocities and can be defined by the condition that the velocities on the free surface must be small compared to $\sqrt{\frac{\Delta p}{\rho}}$ or unity in the nondimensional form.

Consider a bubble in its early stage of collapse. Bernoulli's equation (II-16) gives an estimate for the time derivative of the potential at points on the free surface;

$$\frac{\partial \varphi}{\partial t} = 1 - \frac{1}{2} v^2 = 1 + O(v^2) \quad . \tag{III-63}$$

Now consider any point on the free surface during the interval $t_n < t < t_n + \Delta t$. Let $\vec{v}_n$ be its velocity at $t = t_n$. The rate of change of the i'th component of the velocity of the point is

$$\frac{Dv_i}{Dt} = \frac{\partial v_i}{\partial t} + \vec{v} \cdot \nabla v_i \approx \frac{\partial v_i}{\partial t} + \vec{v}_n \cdot \nabla v_i$$

$$\approx \left(\frac{\partial}{\partial t} + \vec{v}_n \cdot \nabla \right) \frac{\partial \varphi}{\partial x_i} \quad . \tag{III-64}$$

Since $\vec{v}_n$ is a constant, Eq. (III-64) may be written as

$$\frac{Dv_i}{Dt} \approx \frac{\partial}{\partial x_i} \left(\frac{\partial \varphi}{\partial t} + \vec{v}_n \cdot \nabla \varphi \right) \tag{III-65}$$

$$\approx \frac{\partial}{\partial x_i} \left(\frac{\partial \varphi}{\partial t} + O(v^2) \right) \approx \frac{\partial}{\partial x_i} \left(\frac{\partial \varphi}{\partial t} \right) \quad . \tag{III-66}$$

Since $\frac{\partial \varphi}{\partial t}$ satisfies Laplace's equation throughout the liquid and approaches zero infinitely far from the bubble, comparison of Eqs. (III-63)

and (III- 2) shows that

$$\frac{\partial \varphi}{\partial t} = \frac{\varphi}{t} + O(v^2), \quad \text{throughout the liquid.} \tag{III-67}$$

Substitution of Eq. (III-67) into (III-66) produces

$$\frac{Dv_i(t)}{Dt} \approx \frac{v_i(t)}{t} \quad . \tag{III-68}$$

Equation (III-68) provides an estimate of how the velocity changes during time steps in the early stage of collapse. Using this estimate in place of the approximation that the velocity remains constant, modified forms of Eqs. (III-1) and (III-3) can be found. Integration of Eq. (III-68) from $t = t_n$ gives

$$\vec{v} \approx t \frac{\vec{v}_n}{t_n} \quad \text{for} \quad t_n \leq t \leq t_n + \Delta t_n \quad . \tag{III-69}$$

then

$$\Delta \vec{x} = \int_{t_n}^{t_n+\Delta t_n} \vec{v}\, dt \approx \frac{\frac{1}{2}\left[(t_n+\Delta t_n)^2 - t_n^2\right]}{t_n} \vec{v}_n \tag{III-70}$$

and

$$\Delta \varphi = \int_{t_n}^{t_n+\Delta t_n} \left(1 + \frac{1}{2} v^2\right) dt \approx \Delta t_n + \frac{\frac{1}{6}\left[(t_n+\Delta t_n)^3 - t_n^3\right]}{t_n^2} |\vec{v}_n|^2 \quad . \tag{III-71}$$

Note that Eqs. (III-70) and (III-71) reduce to Eqs. (III-1) and (III-3) as $\frac{\Delta t_n}{t_n}$ becomes smaller. They also reduce to Eqs. (III-61) and (III-62) as $t_n \to 0$ and $\frac{\vec{v}_n}{t_n} \to \vec{V}$.

In the improved method the initial time step is made using

Eqs. (III-61) and (III-62). The time steps immediately following the initial time step are then made using Eqs. (III-70) and (III-71). With this method the initial time step does not need to be large to insure the accuracy of the following time steps. The sizes of the time steps are steadily reduced throughout the early stage of collapse to compensate for the increasing error in approximation (III-69). This approximation remains of some value even as late as $t = 0.40$. Later time steps are based on Eqs. (III-1) and (III-3).

Equation (III-67) indicates that the potential increases linearly in time during the early stage of collapse. When a time step in the early stage of collapse takes its initial potentials and outer boundary potentials from the previous time step, it is worthwhile to multiply these potentials by a factor reflecting this increase with time.

IV. COLLAPSE NEAR A SOLID WALL

A. Results of Numerical Simulation

The collapse of an initially spherical bubble near a plane solid wall was simulated for two cases. In Case 1 the parameter $\frac{b}{R_o}$ was unity; that is the bubble boundary was in contact with the solid wall and tangent to it. In Case 2 $\frac{b}{R_o}$ was 1.5; the closest distance from the bubble boundary to the solid wall was initially half the radius of the bubble. Ninety-four time steps were used for Case 1 and seventy-seven for Case 2. Calculations were stopped when the liquid jet reached the opposite wall of the bubble since the assumption of incompressibility is no longer valid. The bubble shapes for selected time steps from Cases 1 and 2 are shown superimposed in Figs. 8 and 9, respectively. Table V lists the time interval from the initiation of collapse for each shape and the downward velocity on the upper portion of the bubble at the axis of symmetry. The time intervals, which are scaled like $R_o\sqrt{\frac{\rho}{\Delta p}}$, are given in units of $R_o(\rho/\Delta p)^{\frac{1}{2}}$. The velocities, which are scaled like $\sqrt{\frac{\Delta p}{\rho}}$, are given in m/sec for the special value

$$\frac{\Delta p}{\rho} = \frac{10^6 \text{ dynes/cm}^2}{1.0 \text{ g/cm}^3} \approx \frac{1 \text{ atm.}}{\text{density of water}} \quad . \qquad \text{(IV-1)}$$

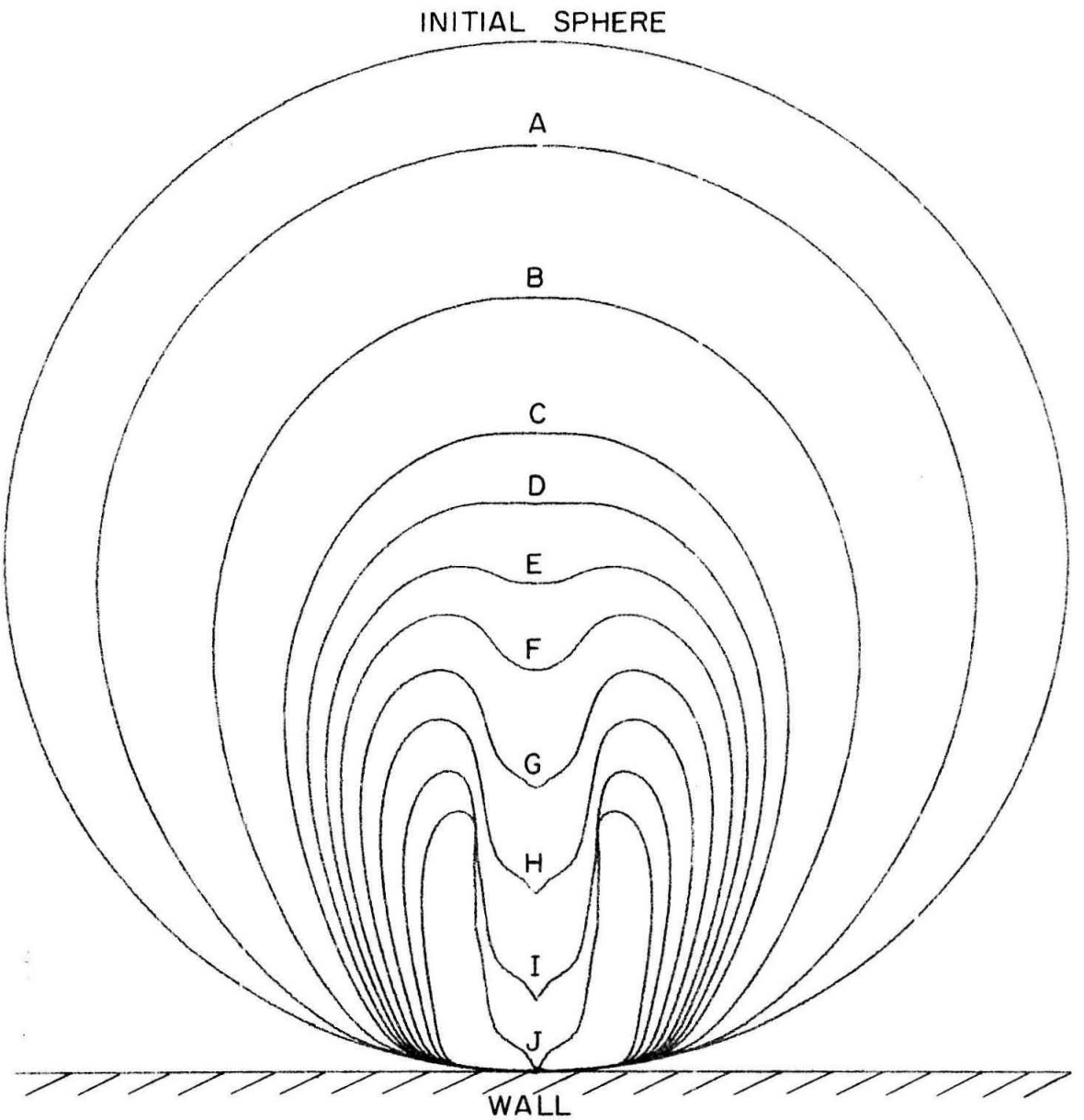

Fig. 8 Bubble Surfaces from Case 1

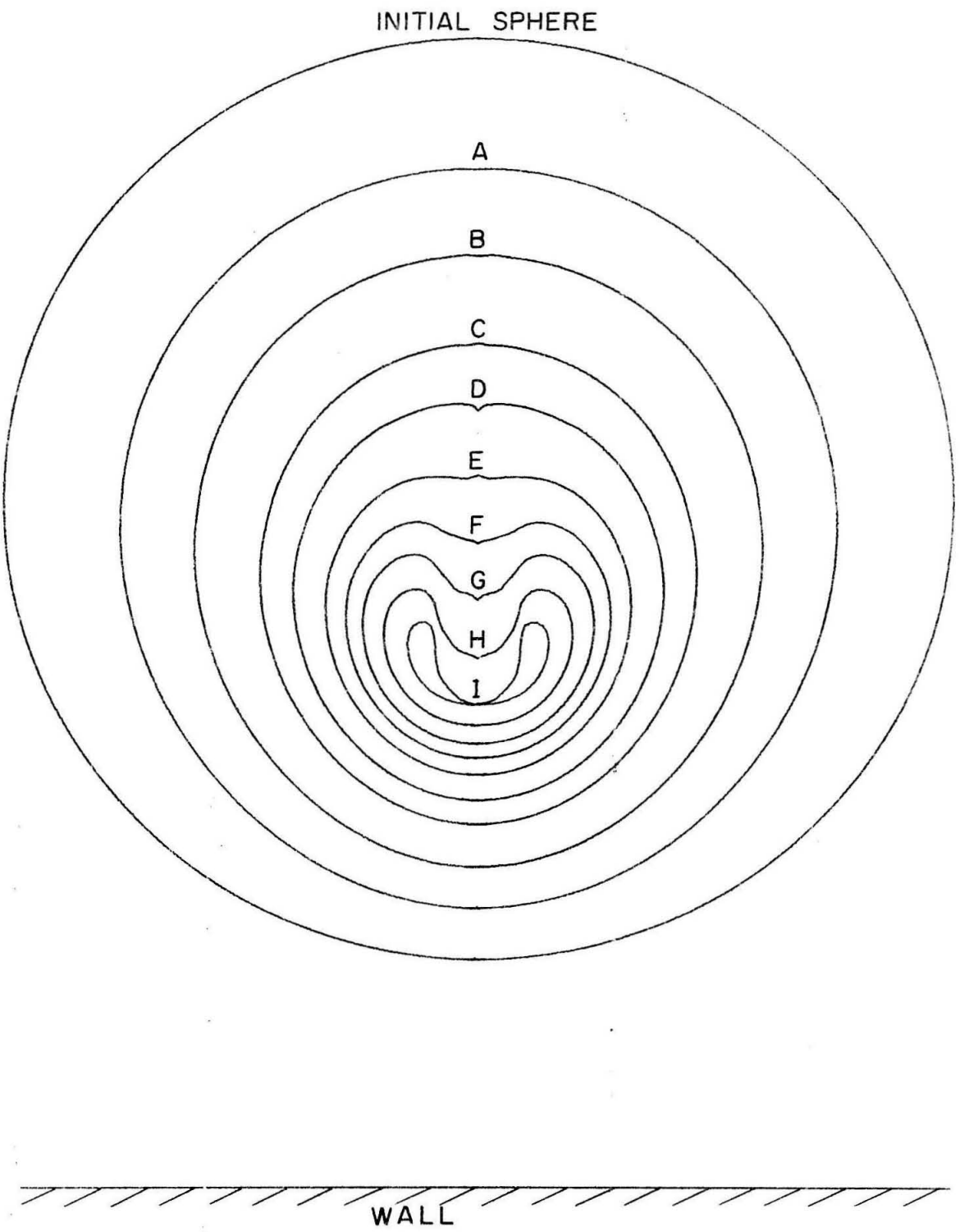

Fig. 9 Bubble Surfaces from Case 2

TABLE V

Time Interval from Initiation of Collapse and the Velocity of the Bubble Boundary at the Axial Point most distant from the Wall for the Cases Illustrated in Fig. 8 and Fig. 9

	Figure 8		Figure 9	
Shape	Time	Velocity	Time	Velocity
A	0.63	7.7 m/sec	0.725	10 m/sec
B	0.885	19 m/sec	0.875	17 m/sec
C	0.986	42 m/sec	0.961	35 m/sec
D	1.013	65 m/sec	0.991	53 m/sec
E	1.033	100 m/sec	1.016	94 m/sec
F	1.048	125 m/sec	1.028	142 m/sec
G	1.066	129 m/sec	1.036	160 m/sec
H	1.082	129 m/sec	1.044	165 m/sec
I	1.098	128 m/sec	1.050	170 m/sec
J	1.119	128 m/sec		

Selected shapes for Case 1 are shown individually in Figs. 10, 11, and 12; shapes for Case 2 are shown in Figs. 13, 14, and 15. Potentials and the two velocity components at lettered points on the bubble boundary are listed in table VI and VII. The potentials, which are scaled like $R_o\sqrt{\frac{\Delta p}{\rho}}$, are listed in their nondimensional form. The velocities are given in m/sec assuming the special value of Eq. (IV-1).

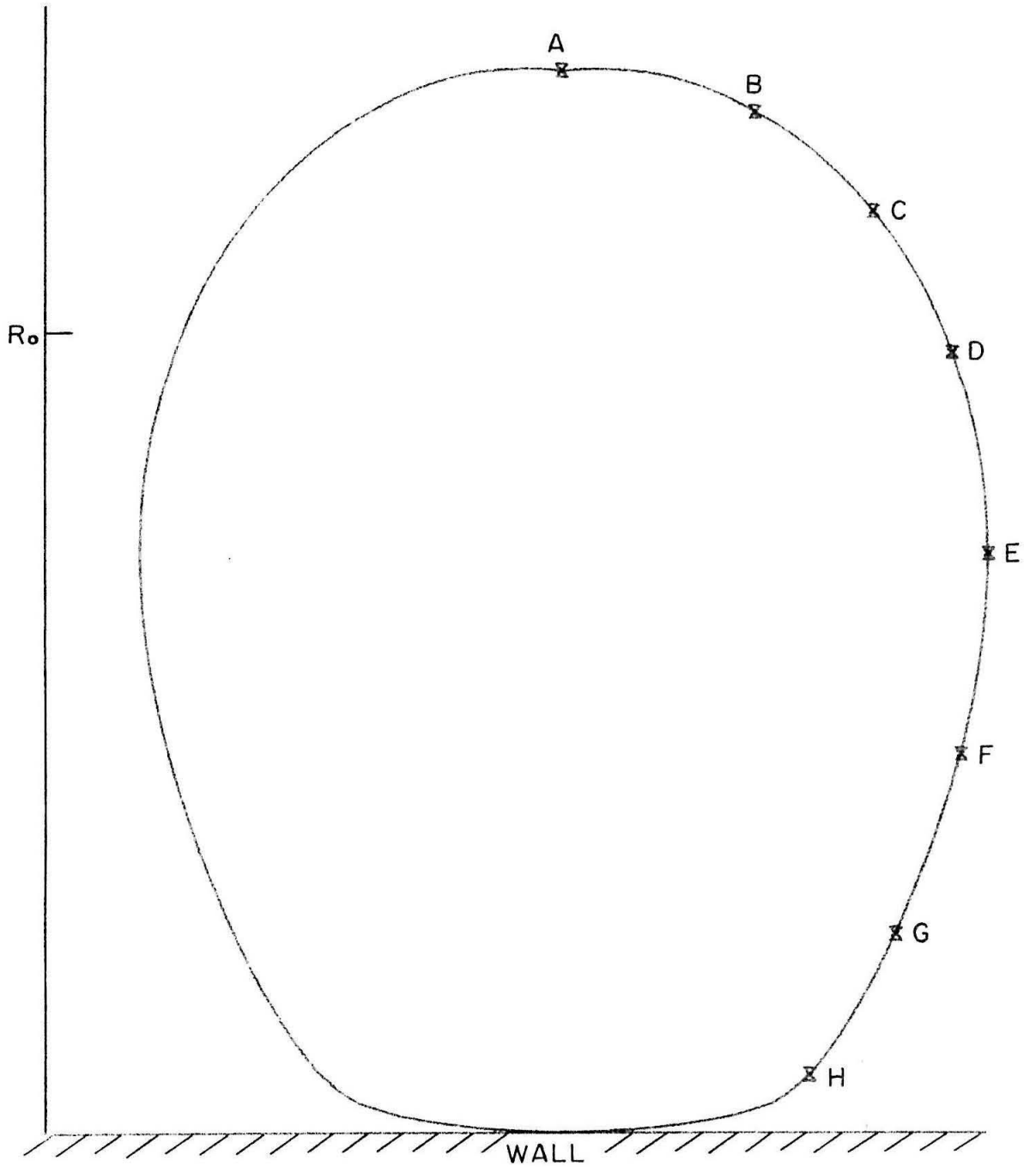

Fig. 10 Bubble Surface from Case 1 at t = 0.96

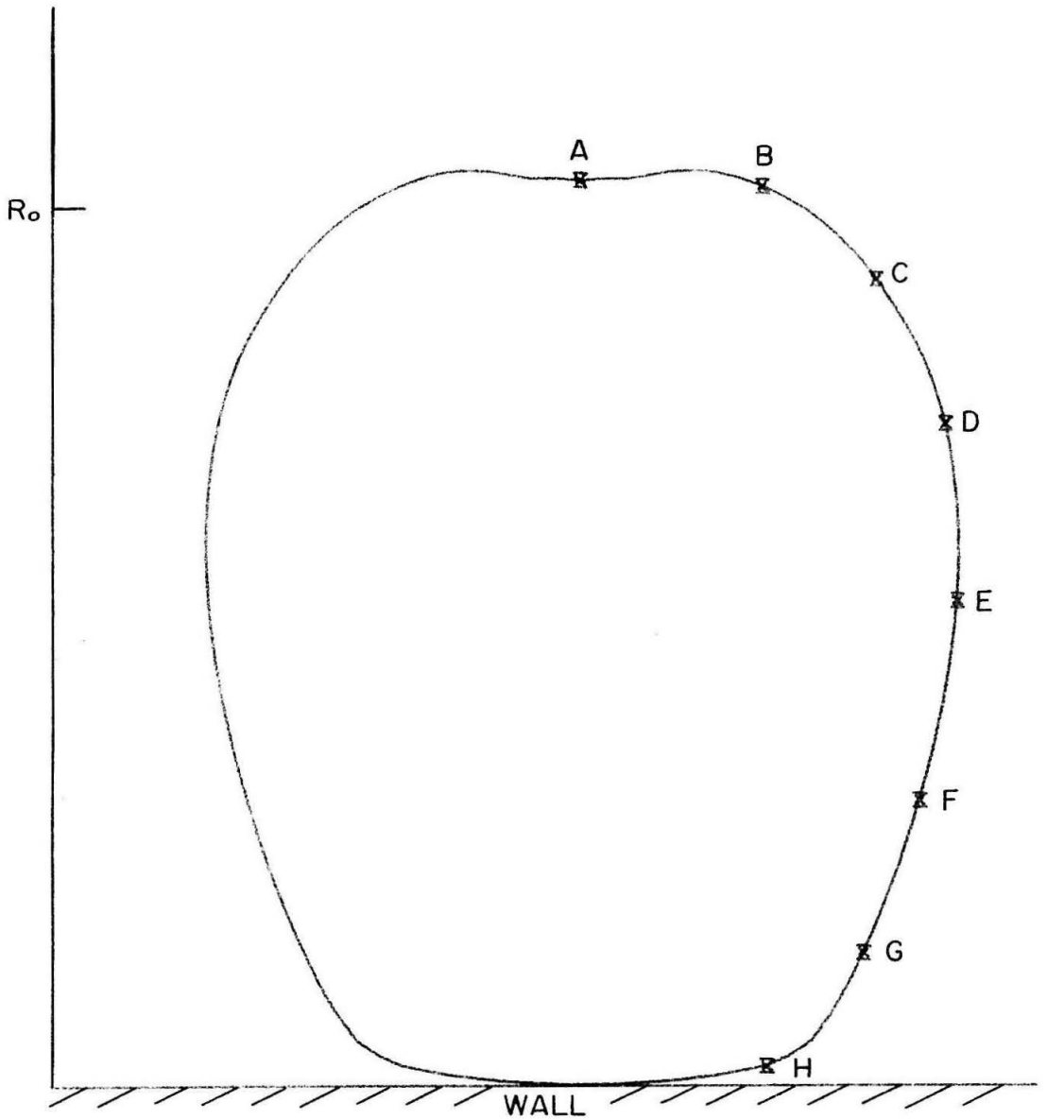

Fig. 11 Bubble Surface from Case 1 at t = 1.024

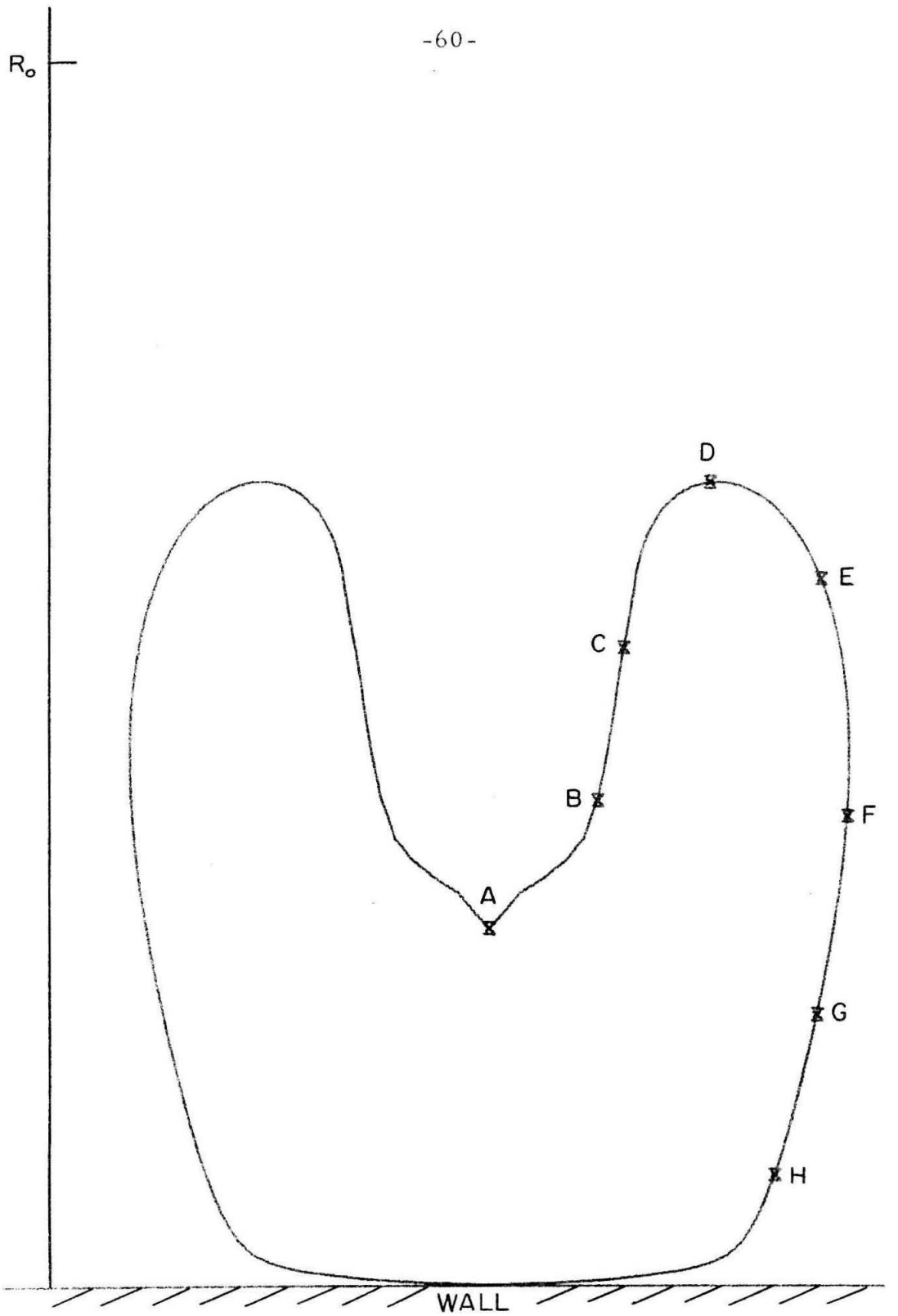

Fig. 12 Bubble Surface from Case 1 at t = 1.086

TABLE VI

Potentials and Velocities of Selected Free Surface Points in Case 1

Bubble Surface in Fig. 10

Point	Potential	Vertical Velocity	Horizontal Velocity	Point	Potential	Vertical Velocity	Horizontal Velocity
A	1.400	-31 m/s	0.0 m/s	E	1.109	3.3 m/s	-14 m/s
B	1.334	-23 m/s	-17 m/s	F	1.036	4.9 m/s	-9.3 m/s
C	1.275	-13 m/s	-21 m/s	G	.986	4.3 m/s	-5.5 m/s
D	1.207	-3.1 m/s	-20 m/s	H	.962	2.2 m/s	-1.5 m/s

Bubble Surface in Fig. 11

A	2.314	-82 m/s	0.0 m/s	E	1.167	5.6 m/s	-15 m/s
B	1.731	-38 m/s	-41 m/s	F	1.085	5.7 m/s	-9.9 m/s
C	1.458	-9.1 m/s	-34 m/s	G	1.041	4.6 m/s	-5.9 m/s
D	1.280	2.2 m/s	-24 m/s	H	1.024	0.4 m/s	-0.1 m/s

Bubble Surface in Fig. 12

A	6.688	-129 m/s	0.0 m/s	E	1.431	.8 m/s	-44 m/s
B	5.379	-124 m/s	-0.7 m/s	F	1.239	7.8 m/s	-23 m/s
C	3.822	-124 m/s	-1.9 m/s	G	1.158	7.6 m/s	-16 m/s
D	1.901	-77 m/s	-73 m/s	H	1.106	6.9 m/s	-10 m/s

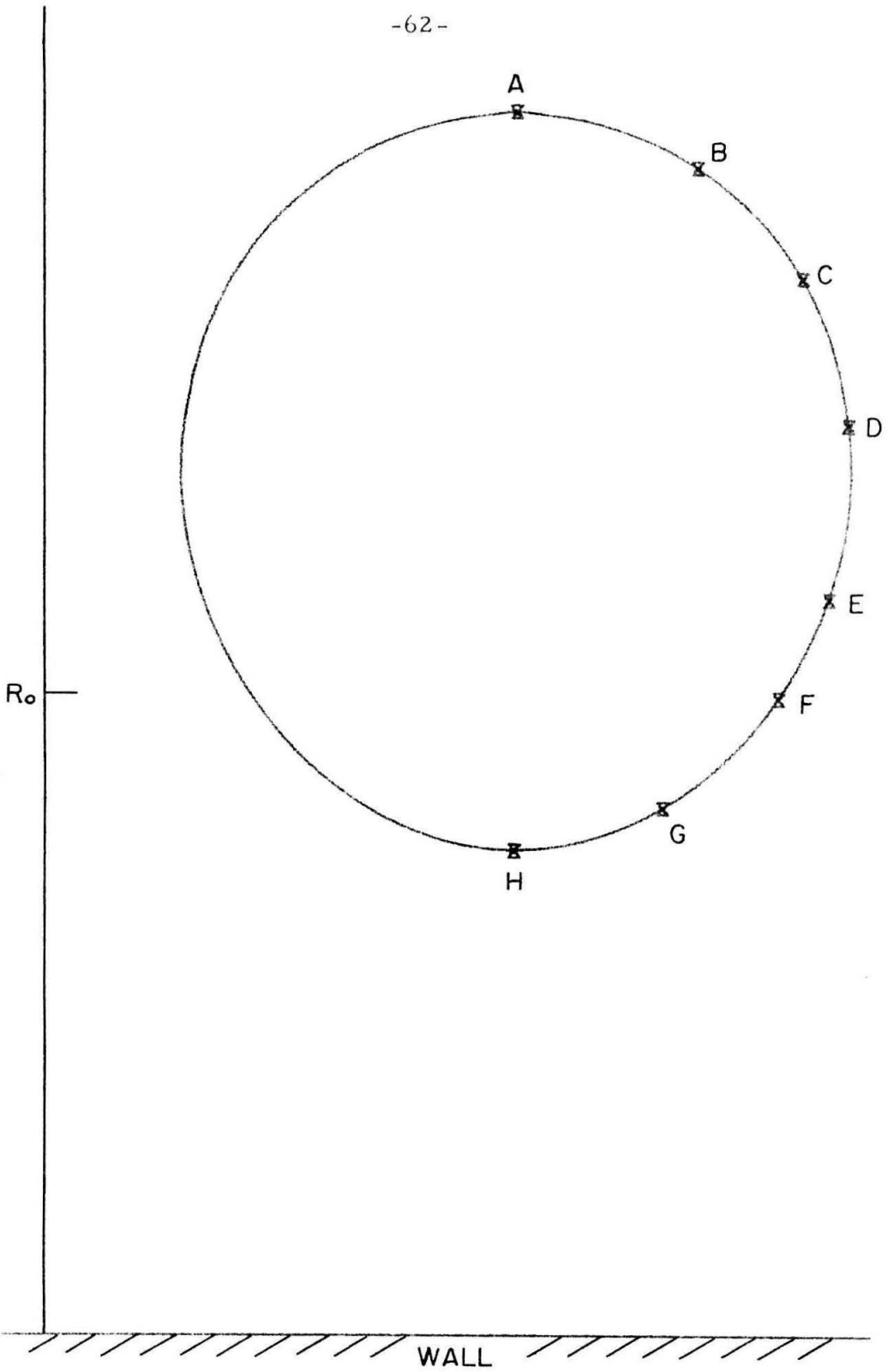

Fig. 13 Bubble Surface from Case 2 at $t = 0.935$

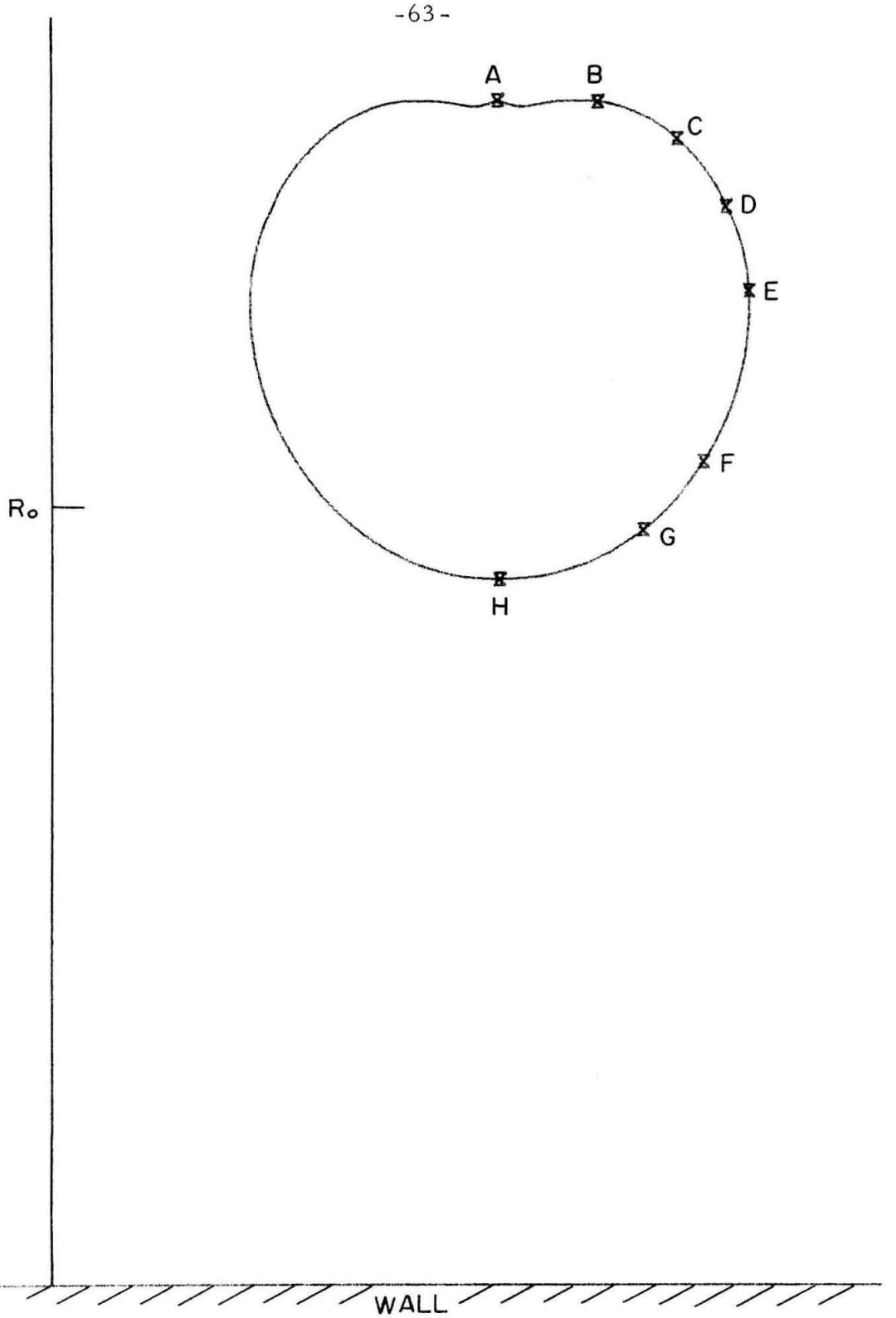

Fig. 14 Bubble Surface from Case 2 at t = 1.019

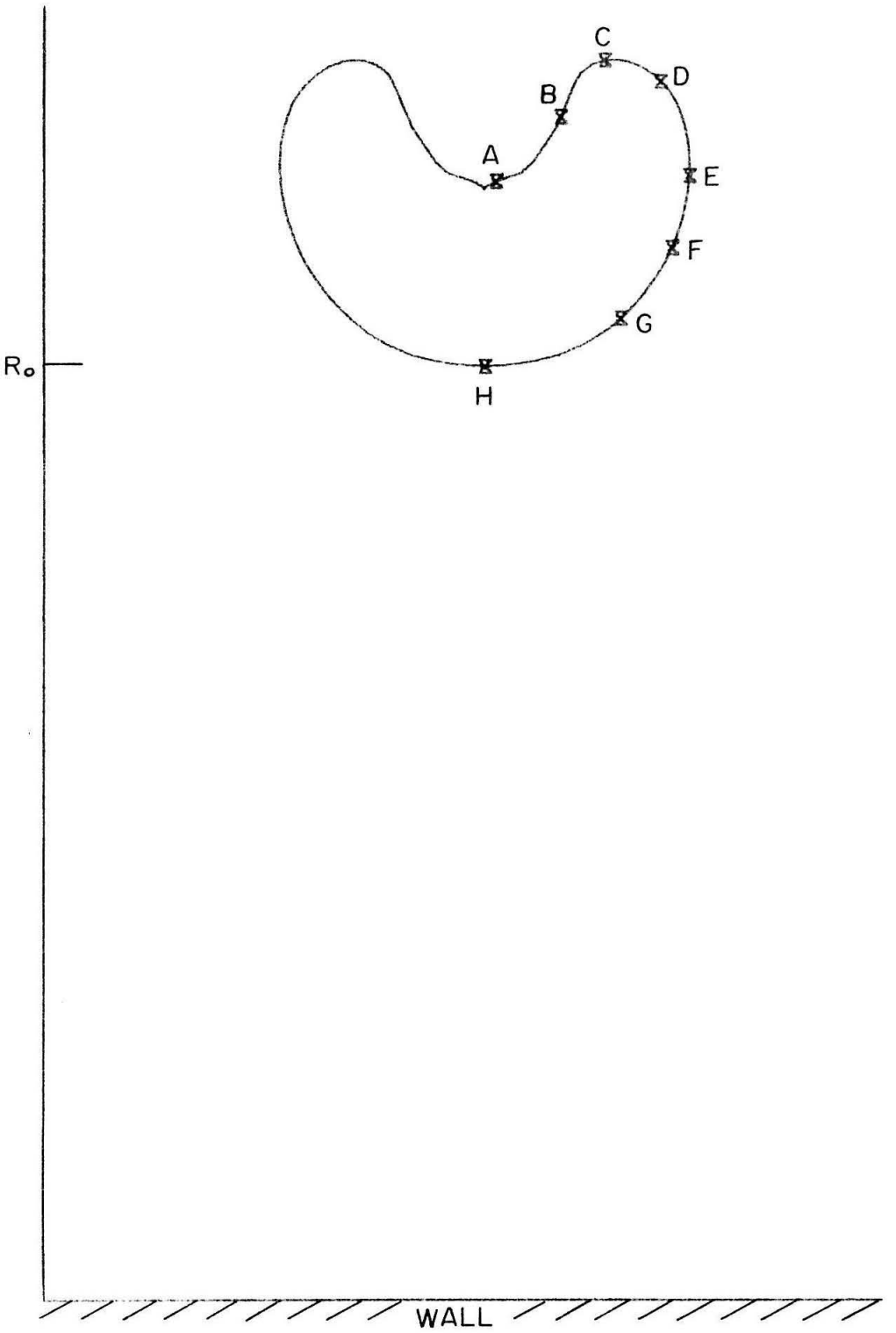

Fig. 15 Bubble Surface from Case 2 at $t = 1.042$

TABLE VII

Potentials and Velocities of Selected Free Surface Points in Case 2

Bubble Surface in Fig. 13

Point	Potential	Vertical Velocity	Horizontal Velocity	Point	Potential	Vertical Velocity	Horizontal Velocity
A	1.254	-25 m/s	0.0 m/s	E	1.084	7.1 m/s	-14 m/s
B	1.236	-19 m/s	-15 m/s	F	1.051	8.9 m/s	-10 m/s
C	1.198	-9 m/s	-20 m/s	G	1.016	10 m/s	-5.8 m/s
D	1.150	0.0 m/s	-19 m/s	H	1.005	12 m/s	0.0 m/s

Bubble Surface in Fig. 14

A	2.324	-108 m/s	0	E	1.377	10 m/s	41 m/s
B	2.043	-79 m/s	-47 m/s	F	1.273	18 m/s	-22 m/s
C	1.720	-29 m/s	-55 m/s	G	1.240	22 m/s	-16 m/s
D	1.543	-6.5 m/s	-46 m/s	H	1.232	29 m/s	0.0 m/s

Bubble Surface in Fig. 15

A	4.740	-164 m/s	2 m/s	E	1.551	19 m/s	-60 m/s
B	3.600	-170 m/s	-40 m/s	F	1.465	29 m/s	-46 m/s
C	2.337	-140 m/s	-96 m/s	G	1.416	39 m/s	-33 m/s
D	1.839	-30 m/s	-101 m/s	H	1.425	56 m/s	0.0 m/s

The pressure in the liquid at the solid wall was calculated at the axis of symmetry in Case 2. It was found to rise steadily from an initial value of $-.92\Delta p$ below ambient to about $14\Delta p$ above ambient pressure at the time the jet reaches the opposite boundary of the bubble.

B. Discussion of Results

The solid wall influences the bubble early in the collapse chiefly by reducing the upward motion of the lower portion of the bubble. As a result the bubble becomes elongated in the direction normal to the wall as was predicted by Rattray[3]. The bottom of the bubble still moves upward towards the bubble center in Case 2, but since this upward motion is reduced, the centroid of the bubble moves towards the wall displaying the well-known Bjerknes effect.

As the bubble acquires kinetic energy, this energy is concentrated in the upper portion of the bubble which eventually flattens and forms a jet. Once the jet is formed, the speed of its tip remains fairly constant. It may be argued intuitively that when a liquid jet is bounded mainly by a free surface at constant pressure, most of the liquid in the jet will be near this constant pressure. Since the pressure gradient is small, the acceleration should also be small.

The behavior of the upper portion of the bubble in Case 2 is not very different from Case 1. The overall shapes appear quite different, however, because the bottom of the bubble must remain in contact with the solid wall in Case 1 but is allowed mobility in Case 2. The jet speed in Case 2 (about 170 m/sec under atmospheric Δp) is somewhat larger than the speed in Case 1 (about 130 m/sec). This behavior is as

expected since a bubble which is farther from the wall collapses with less distortion and can concentrate its energy over a smaller volume. Note that after jet formation the bubble volume, excluding the jet, is greater in Case 1 than in Case 2.

The jet appears to be the result of the deformation caused by the presence of the wall during the early part of the collapse rather than the influence of the wall at the time of the jet formation. It is known from the theory of Plesset and Mitchell that a small deformation can lead to jetting later in the collapse. In Case 2 the bubble is too many radii from the wall at the time the jet is formed for the wall to have an important influence on the flow near the bubble surface.

It should be remembered that in most situations the bubble can collapse under a pressure momentarily greater than atmospheric producing higher speeds. A magnetostrictive oscillator at the California Institute of Technology, for example, produces a periodic pressure amplitude of about ten atm[4]. This oscillator has a natural frequency of 15×10^3 cycles per second corresponding to a wavelength of about ten cm. in water. Since the total collapse time for both Case 1 and Case 2 is roughly $R_o\sqrt{\frac{\rho}{\Delta p}}$, bubbles with initial radii of the order of 10^{-2} cm or less experience a nearly constant local pressure as they collapse. Pressure gradients are unimportant for these particular bubbles since the wavelength is so much larger than their radii; their collapses are driven by the local pressure.

The effects of additional nonspherical influences such as a distorted initial shape should, in general, decrease the jet speed by increasing the asymmetry of the collapse. It is possible, however,

that a bubble may have an asymmetry that partially cancels the effect of the wall allowing the bubble to concentrate more of its energy in a faster jet.

Although the bubble is initially quite close to the wall in Case 2, the final jet must pass through the liquid for a distance of more than five times its diameter before it reaches the solid wall. The jet in Case 1, which strikes the wall directly, seems the more capable of damage. Apparently these bubbles must almost touch the wall initially to be capable of damaging it.

A jet of speed v directly striking a solid boundary produces an initial pressure given by the water hammer equation[18],

$$p_{WH} = \rho_L c_L v \left(\frac{\rho_s c_s}{\rho_L c_L + \rho_s c_s} \right) \qquad \text{(IV-2)}$$

where the L and s subscripts refer to the liquid and the solid, respectively. Usually $\rho_s c_s$ is large compared to $\rho_L c_L$ producing the approximation

$$p_{WH} \approx \rho_L c_L v \quad .$$

A speed of 130 m/sec, for example, corresponds to an impact stress of about 2000 atm.

Experiments by Hancox and Brunton[18] have shown that multiple impacts by water at a speed of 90 meters/sec can erode even stainless steel. They mounted specimens on the rim of a rotating wheel so that the specimen would pass through a stream of water once every rotation. Approximately 4×10^5 impacts were required to produce erosion pits on a specimen of 18/8 austenitec stainless steel with

an initial average scratch depth of 12μm or greater. The jet was 1.3 mm in diameter for this experiment.

Hancox and Brunton suggested that the small surface depressions, which are the first sign of erosion in metals, are caused by local yielding at soft spots on the surface. This, they believed, explains why a stainless steel with an average yield strength of 11,000 Kg/cm^2 erodes at a velocity of 90 m/sec corresponding to a water hammer pressure of 1,300 Kg/cm^2.

Benjamin and Ellis present two series of photographs of bubbles collapsing near a solid wall in Figs. 3 and 4 of their paper. The collapse illustrated in Benjamin and Ellis' Fig. 4 is very similar to Case 2 in this thesis. The collapse illustrated in their Fig. 3 falls between Case 1 and Case 2. Benjamin and Ellis estimated the jet speed in their Fig. 3 to be about 10 m/sec. During collapse they maintained an ambient pressure of about 0.04 atm. The vapor pressure of the water is very important at this reduced pressure. Since Benjamin and Ellis did not mention the temperature of the water, this pressure cannot be determined directly. However, Δp can be deduced from the total collapse time which they gave as 10 ms. The total collapse time for a spherical bubble is, according to Rayleigh,

$$\tau = 0.915\, R_o \sqrt{\frac{\rho}{\Delta p}} \quad . \qquad \text{(IV-3)}$$

The total collapse times for Cases 1 and 2 are only slightly greater since most of the time is consumed early in the collapse while the bubble is nearly spherical. For collapse near a solid wall, then, the total collapse time is roughly

$$\tau \approx R_o \sqrt{\frac{\rho}{\Delta p}} \quad * \qquad . \qquad \text{(IV-4)}$$

Since $R_o \approx 1.0$ cm. and $\tau = 10$ ms, the pressure difference for the collapse in Fig. 3 of Benjamin and Ellis is roughly

$$\Delta p = p_\infty - p_v \approx 10^4 \text{ dynes/cm}^2 \approx .01 \text{ atm.} \qquad \text{(IV-5)}$$

A vapor pressure of 0.03 atm. corresponds to a temperature of about 76°F. Speeds under one atmosphere pressure difference should be increased by a factor of ten giving an estimated jet speed of roughly 100 m/sec so that the experimental observation of Benjamin and Ellis is reconciled with the calculations performed here.

---

* Rattray[3] derived the formula $\frac{\tau}{R_o}\sqrt{\frac{\Delta p}{\rho}} = .915\left(1 + 0.41\ \frac{R_o}{2b}\right) + O\left(\frac{R_o}{2b}\right)^2$ from his perturbation analysis.

V. COLLAPSE OF INITIALLY NONSPHERICAL BUBBLES

A. Results of Numerical Simulation

Two cases of initially nonspherical bubbles collapsing in a homogeneous liquid were simulated. For the first of these (Case 3) the initial bubble shape, described by its radius

$$r_s(\theta, 0) = 1 + \frac{1}{10} P_2(\cos\theta) \quad , \qquad (V\text{-}1)$$

was roughly that of a prolate ellipsoid. The other case (Case 4) had an oblate initial shape with a radius of

$$r_s(\theta, 0) = 1 - \frac{1}{10} P_2(\cos\theta) \quad . \qquad (V\text{-}2)$$

The liquid was assumed to be initially at rest in both cases. A total of seventy-six time steps were used for Case 3 and eighty-six for Case 4.

Bubble shapes for selected time steps for Cases 3 and 4 are shown superimposed in Fig. 16 and 17, respectively. Table VII lists the time from the initiation of collapse for all of these shapes. The velocity of the bubble surface on the plane of symmetry and on the axis of symmetry is also listed for each shape. As in Table V, the velocities are given for the conditions specified in Eq. (IV-1) and the times are listed in nondimensional form.

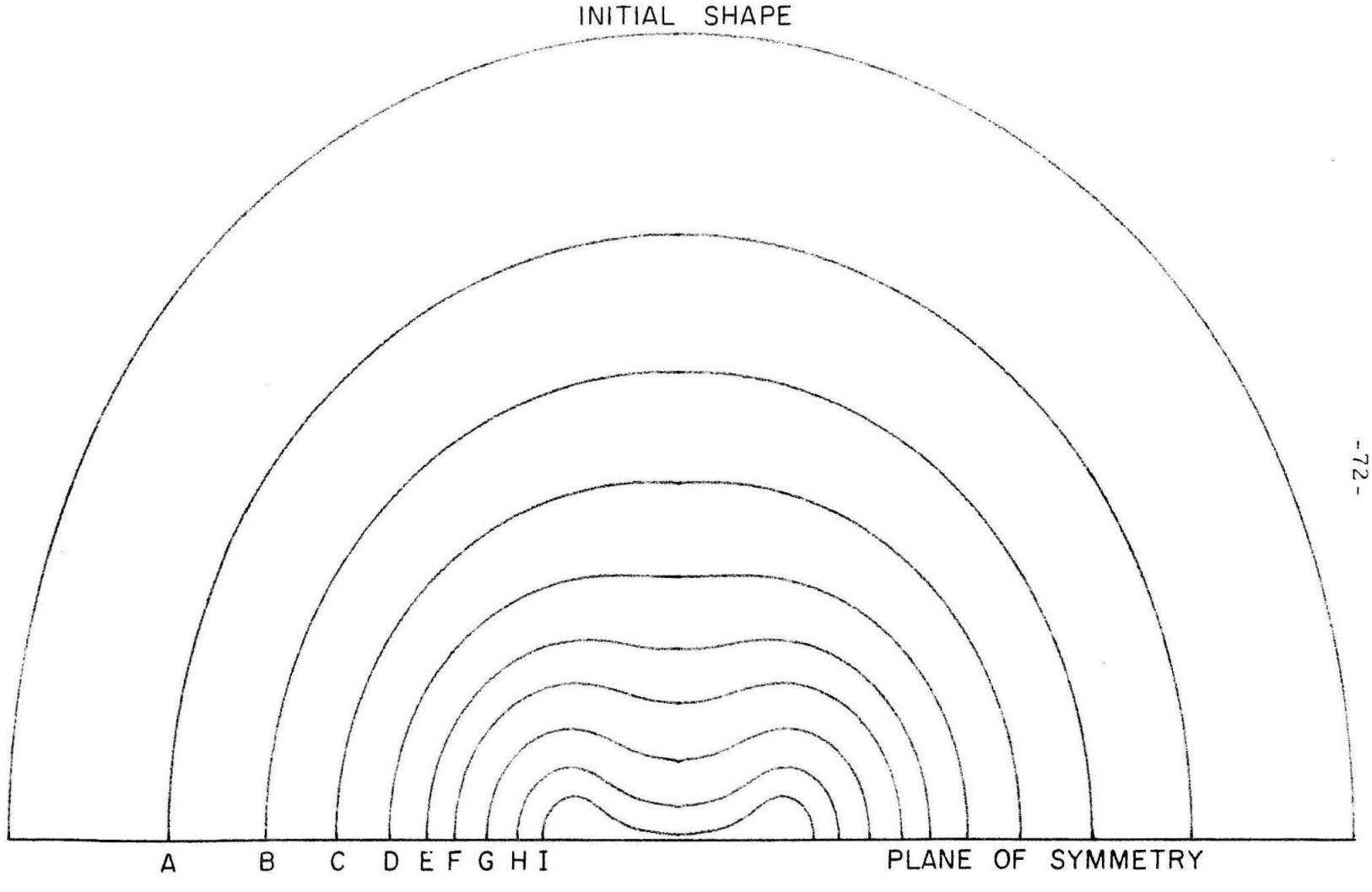

Fig. 16 Bubble Surfaces from Case 3

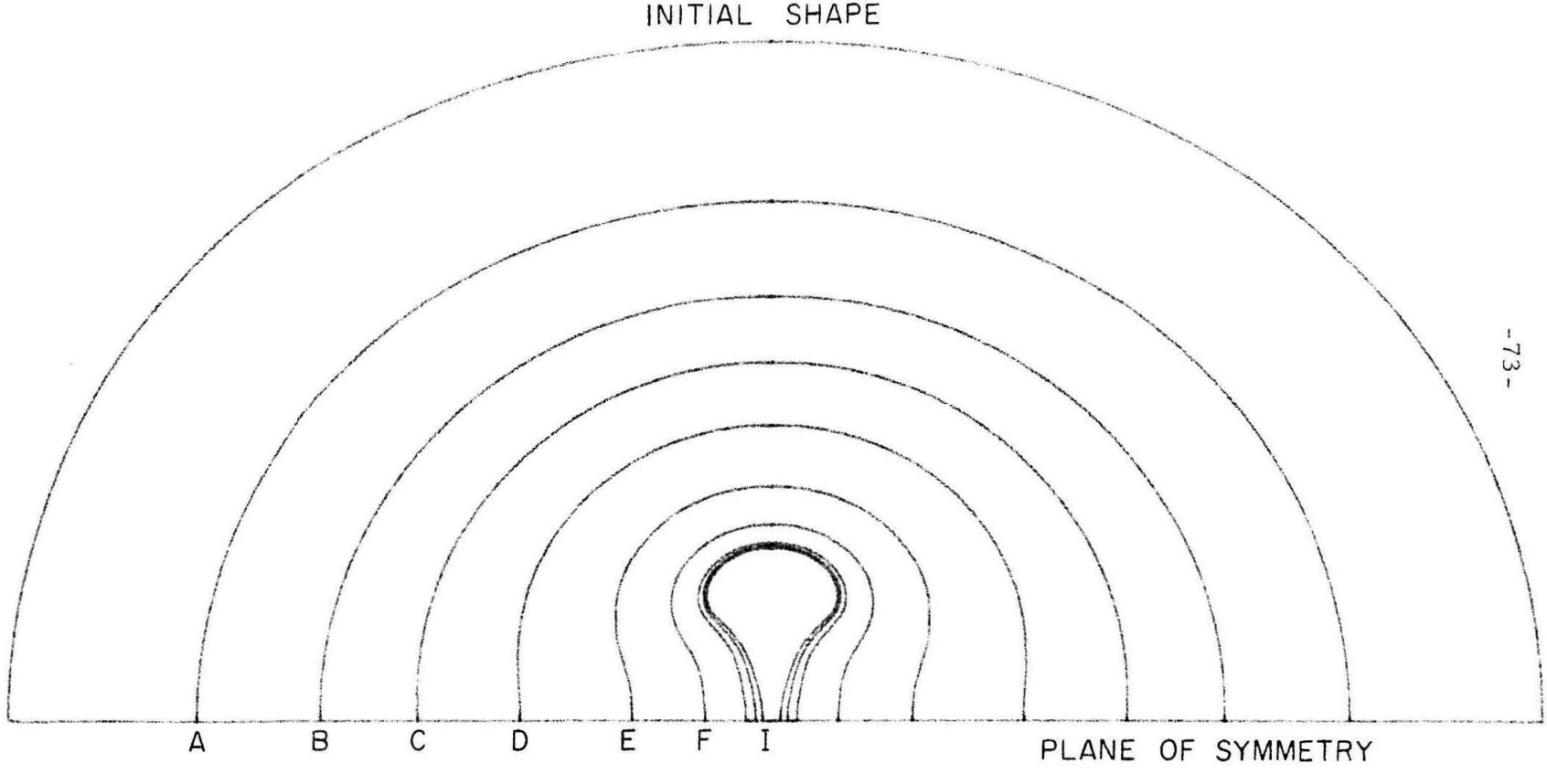

Fig. 17 Bubble Surfaces from Case 4

TABLE VIII

Time Intervals from Initiation of Collapse, and Velocities of the Bubble Surface on the Plane of Symmetry and the Axis of Symmetry for Shapes Illustrated in Fig. 16 and Fig. 17

Shapes of Fig. 16

Shape	Time	Velocity	
		On Axis of Symmetry	On Plane of Symmetry
A	.645	11 m/sec	8.7 m/sec
B	.775	20 m/sec	14 m/sec
C	.837	32 m/sec	20 m/sec
D	.871	46 m/sec	26 m/sec
E	.890	63 m/sec	33 m/sec
F	.901	76 m/sec	41 m/sec
G	.911	85 m/sec	54 m/sec
H	.918	93 m/sec	78 m/sec
I	.9225	102 m/sec	119 m/sec

Shapes of Fig. 17

Shape	Time	Velocity	
		On Axis of Symmetry	On Plane of Symmetry
A	.645	8.0 m/sec	11 m/sec
B	.775	12 m/sec	17 m/sec
C	.837	17 m/sec	27 m/sec
D	.879	23 m/sec	42 m/sec
E	.907	38 m/sec	77 m/sec
F	.918	64 m/sec	126 m/sec
G	.9216	85 m/sec	243 m/sec
H	.9221	91 m/sec	336 m/sec
I	.9224	95 m/sec	518 m/sec

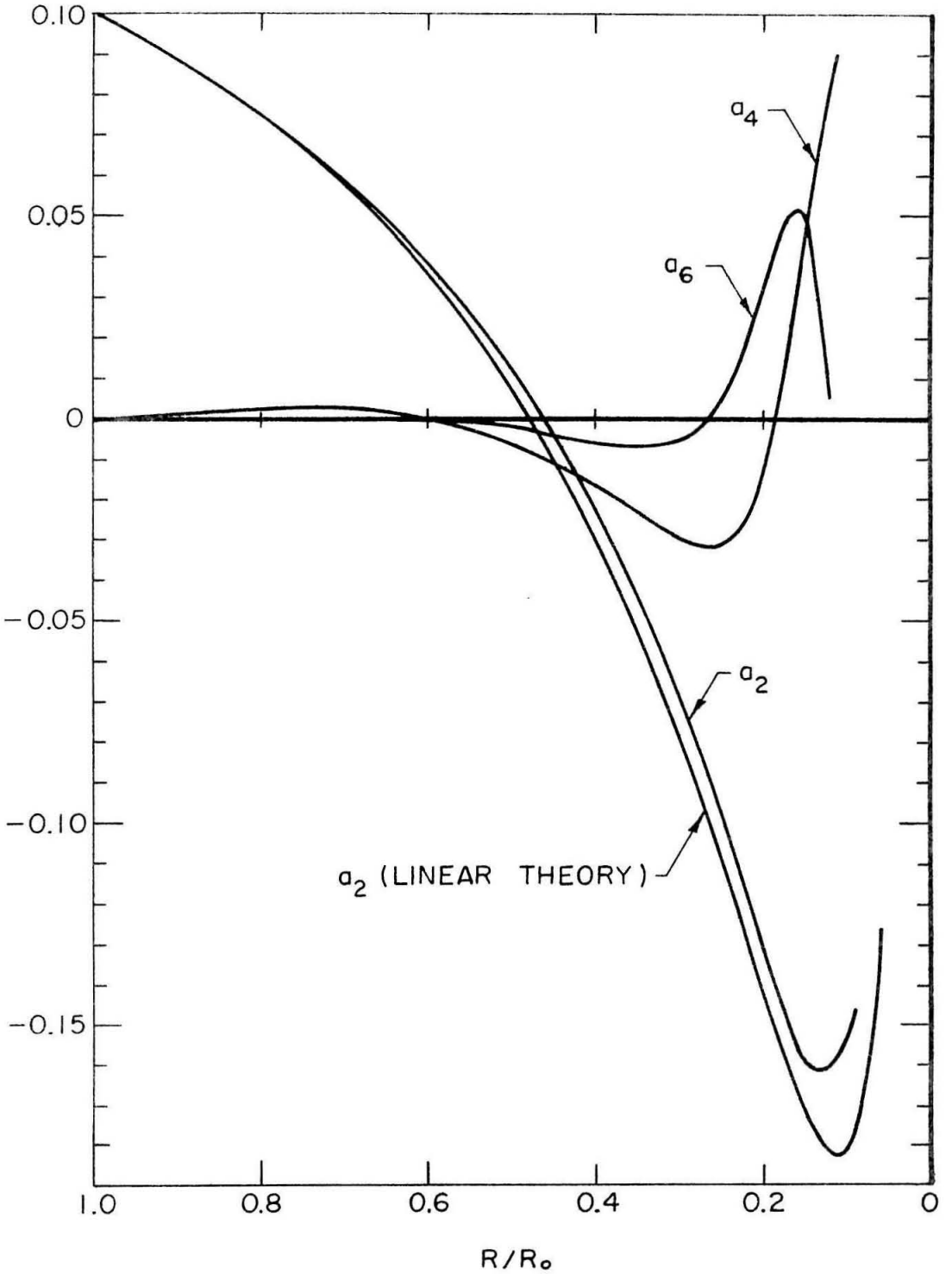

Fig. 1 Coefficients in Expansion of Bubble Radius for Case 3

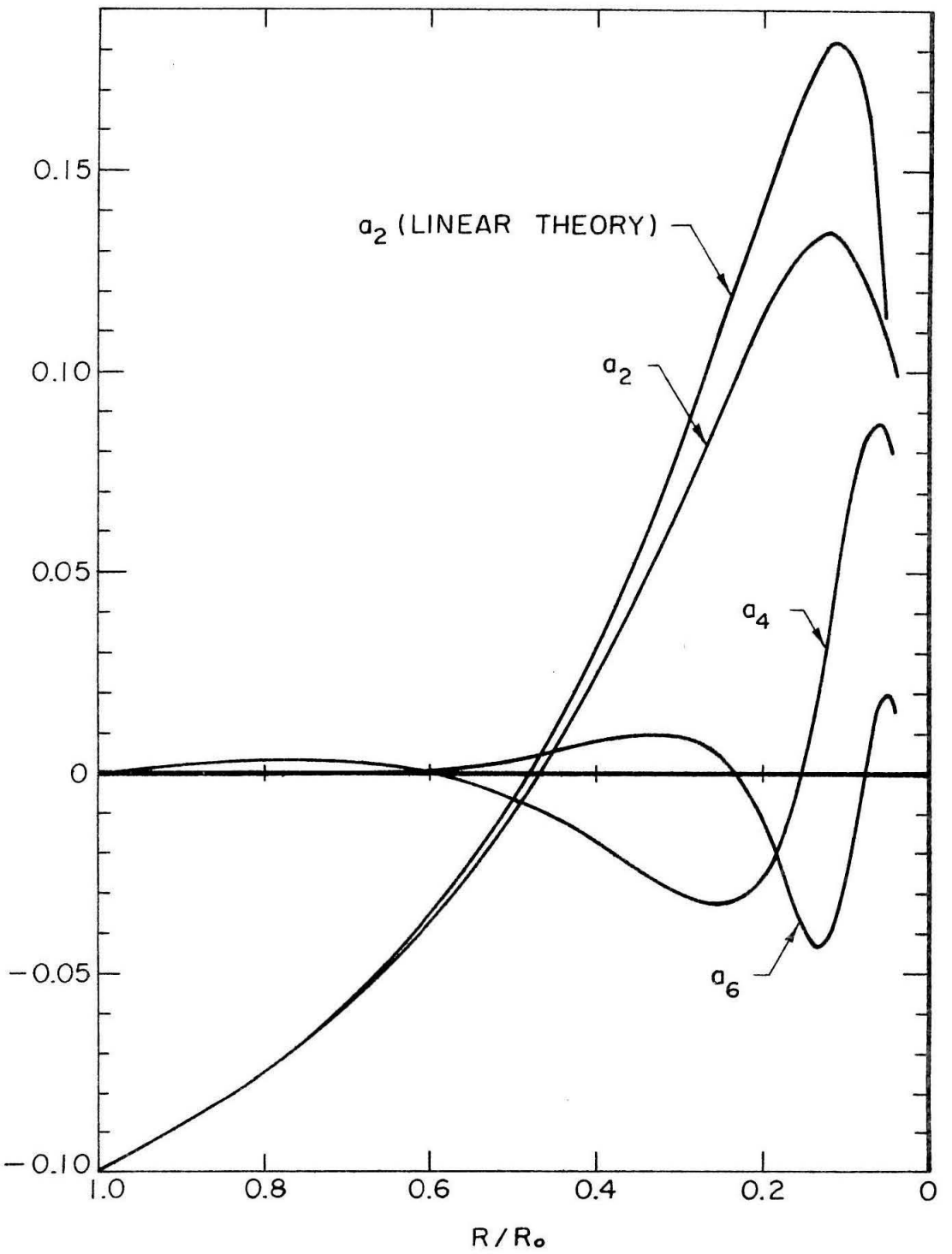

Fig. 19 Coefficients in Expansion of Bubble Radius for Case 4

Since it is of interest to compare the results of numerical simulation with the linear theory, a least squares fit was used for each bubble shape to determine the best values for the mean radius and the coefficients in the expansion

$$r_s(\theta, t) = R(t) + \sum_{n=1}^{5} a_{2n}(t) P_{2n}(\cos\theta) \quad . \qquad (V-3)$$

This fit was successful except for the last few time steps, when the bubble was highly distorted. Figures 18 and 19 show $a_2(t)$, $a_4(t)$, and $a_6(t)$ as functions of $R(t)$. For comparison $a_2(t)$ computed from the linear theory of Plesset and Mitchell is also included.

B. Discussion of Results

The initial elongation of the bubble in Case 3 along its axis causes the velocity on the bubble surface to be greatest at the poles early in the collapse. This eventually causes the formation of jets on the axis of symmetry, which have a velocity of about 100 m/sec under the conditions in Eqs. (IV-1) when they strike. Similarly, the velocity on the bubble surface is a maximum at the plane of symmetry in Case 4 causing the bubble to assume a "dumbbell" shape. As the center of the bubble in Case 4 constricts about the axis, the radial velocity near the plane of symmetry grows indefinitely. This unlimited rise in radial velocity is a result of the assumption of axial symmetry; a small initial distortion lacking axial symmetry would prevent it.

According to the linearized theory, $a_2(t)/a_2(0)$ should follow the same curve for both Case 3 and Case 4, and all other coefficients should remain zero throughout the collapse. The numerical solution

during the first part of the collapse conforms more closely to linear theory than might be expected for an initial distortion of ten percent. During the final part of the collapse, the nonspherical terms in the bubble shape and velocity grow to the order of magnitude of the spherical terms, causing the higher harmonics to be excited. The behavior of $a_4(t)$ closely follows the second order results of Naudé and Ellis[8] (not shown here). Throughout the collapses $a_2(t)$ remains surprisingly close to the linear estimate. The theory of Plesset and Mitchell predicts that $a_2(t)$ will oscillate with increasing frequency as the mean radius approaches zero. The distortion in both cases is large enough, however, so that parts of the bubble strike each other before an entire oscillation can be completed. The main conclusion to be made from these results is that linear theory provides a fairly good representation for this type of collapse.

VI. EVALUATION OF THE NUMERICAL PROCEDURE

A. Accuracy

The accuracy of a solution based on the method of simulation presented here depends on several types of errors. The error left by the Liebmann method in the solution of the potential distribution was discussed in Chapter III. A sufficient number of Liebmann iterations were used in practice to make this error unimportant. Another type of error discussed in Chapter III is the one left by the iterative method used to establish the outer boundary potentials. This error was also unimportant in practice since the changes in the outer boundary potentials between consecutive time steps were well under one percent of the potentials on the free surface, and a single iteration of the outer boundary procedure reduces this error considerably.

Two additional sources of error will be discussed in this Chapter; first, the use of nets of finite mesh length to describe the bubble and the surrounding liquid at a given time and second, the use of finite time steps to obtain the behavior of the bubble as it changes with time. The mesh length is important for the first and last nets of the series. It was pointed out in Chapter III that an insufficient number of free boundary points in the first net can reduce the accuracy of the outer boundary potentials. Comparisons of the potentials before and after the scale of the first net was halved, such as in Table II, indicate that the magnitude of the errors in the outer potentials before the scale change was small compared to the potentials on the free surface. For example, Table II indicates that the errors in the outer boundary

potentials before the scale change combined with the changes between the consecutive time steps were of order 0.003 compared to potentials of order unity on the free surface.

Since, in general, the interpolation between time steps quickly smooths out features the size of a mesh length in the final net or smaller, the mesh length should be kept small compared to the essential features of the bubble. In Fig. 12, for example, point D is a distance of fourteen mesh lengths from the axis of symmetry, and a total of fourty-four free boundary points describe the jet on one side of the axis. Twenty-four free boundary points describe the jet on one side of the axis for surface H in Fig. 16. While the mesh length of the final net can be halved very economically simply by adding another net to the series, the computer time necessary for a collapse is roughly proportional to the number of time steps used. Since this number was kept to a minimum, the errors caused by the use of finite time steps must be carefully examined.

Equations (III-1) and (III-3) are valid if the velocity of the free boundary point, $\vec{v}(t)$, remains constant for $t_n < t < t_n + \Delta t$. If Δt is small, then during the displacement $\vec{v}(t)$ can be approximated by

$$\vec{v}(t) = \vec{v}(t_n) + \frac{\Delta \vec{v}}{\Delta t} (t - t_n) \quad , \tag{VI-1}$$

where

$$\Delta \vec{v} = \vec{v}(t_n + \Delta t) - \vec{v}(t_n) \quad . \tag{VI-2}$$

The displacement of a boundary point, obtained by integration of Eq. (VI-1) is

$$\Delta\vec{x} = \frac{1}{2}\left(\vec{v}(t_n) + \vec{v}(t_n + \Delta t)\right)\Delta t \quad ,$$

$$= \vec{v}_{AV}\Delta t \quad . \tag{VI-3}$$

The change in the potential of the displaced point may be stated in terms of v_{AV} by integrating Eq. (III-2) using Eq. (VI-1) and then neglecting terms of order $(\Delta v)^2$;

$$\Delta\varphi = \left(1 + \frac{1}{2} v_{AV}^2\right)\Delta t \quad . \tag{VI-4}$$

Since $\vec{v}_{AV}$ is not known before the time step, Eqs. (III-1) and (III-3) use the velocity at the beginning of the time step $\vec{v}(t_n)$ instead. Until the jet is formed, the maximum acceleration on the free surface occurs at the axis of symmetry in Cases 1, 2, and 3. An effort was made during this part of the collapse to choose the sizes of the time steps such that the difference between v_{AV} and $v(t_n)$ at the axis of symmetry was less than four percent of v_{AV}. A similar limit was used in Case 4 for the free boundary point on the plane of symmetry. Some insight into how such an error affects the velocities during non-spherical collapse can be gained by examining its effect on spherical collapse. For an upper limit assume

$$v(t_n) = .96\, v_{AV} \quad . \tag{VI-5}$$

Equations (III-1) and (III-3) may be combined for spherical collapse to produce

$$\frac{\Delta\varphi}{\Delta R} = \frac{1}{v(t_n)} + \frac{1}{2} v(t_n) \tag{VI-6}$$

or

$$\frac{\Delta\varphi}{\Delta R} = \frac{1.04}{v_{AV}} + \frac{1}{2}(.96)v_{AV} \quad . \tag{VI-7}$$

To first order in Δv, this difference equation is equivalent to the differential equation

$$\frac{D\varphi}{DR} = \frac{1.04}{v} + \frac{1}{2}(.96)v \quad . \tag{VI-8}$$

For spherical collapse the potential problem at each time step has the solution

$$v = -\frac{\varphi}{R} \quad . \tag{VI-9}$$

Equation (VI-8) may be written as

$$-\frac{D(vR)}{DR} = \frac{1.04}{v} + \frac{1}{2}(.96)v \tag{VI-10}$$

or

$$-\frac{1}{2}\frac{D(v^2)}{DR} = 1.04 + \frac{2.96}{2}v^2 \quad . \tag{VI-11}$$

Integration of this equation produces the solution

$$v = (1.03)\frac{2}{3}\left[\left(\frac{R_o}{R}\right)^{2.96} - 1\right]^{\frac{1}{2}} \tag{VI-12}$$

where v is given in units of $\sqrt{\frac{\Delta p}{\rho}}$ Eq. (VI-12) corresponds to the true solution given by Rayleigh[1],

$$v = \frac{2}{3}\sqrt{\frac{\Delta p}{\rho}}\left[\left(\frac{R_o}{R}\right)^{3} - 1\right]^{\frac{1}{2}} \quad . \tag{VI-13}$$

Thus during the first part of the collapse the velocity for a given bubble radius according to Eq. (VI-12) is about three percent greater than its true value. When R_o/R reaches 2.0, the velocity (under the conditions specified in Eq. (IV-1)) is about 12 m/sec and the net error is

about two percent. The net error becomes zero at $R_o/R = 4.4$ where $v = 65$ m/sec. At $R_o/R = 10$ the velocity is 210 m/sec and the net error is minus two percent. The velocity in Eq. (VI-12) is the velocity calculated as a function of radius and not $\frac{\Delta R}{\Delta t} = v(t_n)$ which is four percent less according to Eq. (VI-5). Thus for any given bubble radius during the first part of the collapse the elapsed time from the initiation of collapse should be about one percent greater than its true value. Since most of the collapse time is consumed before R_o/R becomes large, the error in the total collapse times should not be much greater than one percent.

Although Eq. (VI-12) suggests that the use of finite time steps produces errors of only a few percent in the velocities, it does not indicate exactly how the nonspherical portion of the collapse will be affected. In particular, since the deviation of $a_2(t)$ from the values predicted by linear theory is so small in Cases 3 and 4, it is of interest to know how much of this deviation is actually caused by the use of finite time steps. Therefore, the collapse of a nonspherical bubble satisfying the linearized assumptions was determined using the same time steps employed in Cases 3 and 4. This linearized problem can be solved quite easily, even without the aid of a computer. It is first necessary to find the linearized forms of Eqs. (III-1) and (III-3). The derivation of these forms is roughly parallel to Plesset's derivation of the general linearized equation for $a_n(t)$[6].

In the linearized approximation to Cases 3 and 4, the second harmonic is the only nonspherical term in the radius of the free boundary;

$$r_s(\theta, t) = R(t) + a(t)P_2(\cos\theta) \qquad \text{(VI-14)}$$

It is assumed, of course, that $|a(t)| \ll R(t)$. The potential in the liquid surrounding the bubble is

$$\varphi(d, \theta, t) = \frac{A(t)R(t)}{d} + \frac{B(t)R^3(t)}{d^3} P_2(\cos\theta) \qquad \text{(VI-15)}$$

where d is the distance from the center of the bubble. To first order the potential on the free surface can be written as

$$\varphi[r_s(\theta, t), \theta, t] = A(t) + C(t) P_2(\cos\theta) \qquad \text{(VI-16)}$$

where

$$C = B - \frac{Aa}{R} \quad . \qquad \text{(VI-17)}$$

The radial velocity on the free boundary at $t = t_n$ is to first order

$$\left(\frac{\partial\varphi}{\partial d}\right)_{\substack{d=r_s \\ t=t_n}} = \dot{R}(t_n) + \dot{a}(t_n) P_2(\cos\theta) \qquad \text{(VI-18)}$$

$$= -\frac{A}{R} - \left(\frac{3B}{R} - \frac{2Aa}{R^2}\right) P_2(\cos\theta) \quad . \qquad \text{(VI-19)}$$

Thus at $t = t_n$,

$$\dot{R} = -\frac{A}{R} \qquad \text{(VI-20)}$$

and

$$\dot{a} = -\left(\frac{3C}{R} + \frac{Aa}{R^2}\right) \quad . \qquad \text{(VI-21)}$$

Bernoulli's equation applied on the free surface at $t = t_n$ produces to first order

$$\frac{D\varphi}{Dt} = \frac{\Delta p}{\rho} + \frac{1}{2}\dot{R}^2 + \dot{R}\dot{a} P_2(\cos\theta) + O(\dot{a}^2) \qquad \text{(VI-22)}$$

or

$$\dot{A} = \frac{\Delta p}{\rho} + \frac{1}{2}\dot{R}^2 = \frac{\Delta p}{\rho} + \frac{1}{2}\frac{A^2}{R^2} \qquad \text{(VI-23)}$$

and

$$\dot{C} = \dot{R}\dot{a} = \frac{A}{R}\left(\frac{3C}{R} + \frac{Aa}{R^2}\right) . \qquad \text{(VI-24)}$$

Equations (VI-20) and (VI-21) provide the linearized equivalent of Eq. (III-1):

$$\Delta R = R(t_n+\Delta t_n) - R(t_n) = -\Delta t_n\left(\frac{A}{R}\right)_{t=t_n} \qquad \text{(VI-25)}$$

and

$$\Delta a = a(t_n+\Delta t_n)-a(t_n) = -\Delta t_n\left(\frac{3C}{R} + \frac{Aa}{R^2}\right)_{t=t_n} . \qquad \text{(VI-26)}$$

Equations (VI-23) with $\sqrt{\frac{\Delta p}{\rho}} = 1$ and Eq. (VI-24) provide the linearized equivalent of Eq. (III-3):

$$\Delta A = A(t_n+\Delta t_n) - A(t_n) = \Delta t_n\left(1 + \frac{1}{2}\frac{A^2}{R^2}\right)_{t=t_n} \qquad \text{(VI-27)}$$

and

$$\Delta C = C(t_n+\Delta t_n) - C(t_n) = \Delta t_n\left[\frac{A}{R}\left(\frac{3C}{R} + \frac{Aa}{R^2}\right)\right]_{t=t_n} . \qquad \text{(VI-28)}$$

Similarly, the linearized equations corresponding to Eqs. (III-70) and (III-71) are

$$\Delta R = -\frac{[(t_n+\Delta t_n)^2 - t_n^2]}{2t_n}\left(\frac{A}{R}\right)_{t=t_n} , \qquad \text{(VI-29)}$$

$$\Delta a = -\frac{[(t_n+\Delta t_n)^2 - t_n^2]}{2t_n}\left(\frac{3C}{R} + \frac{Aa}{R^2}\right)_{t=t_n} , \qquad \text{(VI-30)}$$

$$\Delta A = \Delta t_n + \frac{\left[(t_n+\Delta t_n)^3 - t_n^3 \right]}{6t_n^2} \left(\frac{A}{R}\right)^2_{t=t_n} , \qquad \text{(VI-31)}$$

and

$$\Delta c = \frac{\left[(t_n+\Delta t_n)^3 - t_n^3 \right]}{3t_n^2} \left[\frac{A}{R}\left(\frac{3C}{R} + \frac{Aa}{R^2}\right)\right]_{t=t_n} . \qquad \text{(VI-32)}$$

Finally, assuming $\sqrt{\frac{\Delta p}{\rho}} = 1$ and $R_o = 1$, the linearized forms of Eqs. (II-61) and (III-62) are

$$\Delta R = -\frac{1}{2}(\Delta t)^2 , \qquad \text{(VI-33)}$$

$$\Delta a = -\frac{1}{2} a(0)(\Delta t)^2 , \qquad \text{(VI-34)}$$

$$\Delta A = \Delta t\left(1 + \frac{1}{6}(\Delta t)^2\right) , \qquad \text{(VI-35)}$$

and

$$\Delta C = \frac{1}{3}(\Delta t)^3 a(0) . \qquad \text{(VI-36)}$$

The same time steps used in Cases 3 and 4 were applied to Eqs. (VI-25) through (VI-36) to obtain an adjusted linearized solution. The difference between this adjusted linearized solution and the true linearized solution represents the error caused by the use of finite time steps. The adjusted linearized solution is shown with the true linearized solution and the second harmonic determined from the numerical solution in Fig. 20 for Case 3 and in Fig. 21 for Case 4. It is seen that the second harmonic from the numerical solution is even closer to linear theory when the effect of finite time steps is taken into account.

A brief description of the calculation of the true linearized solution which appears in Figs. 18 through 21 may be of interest. As

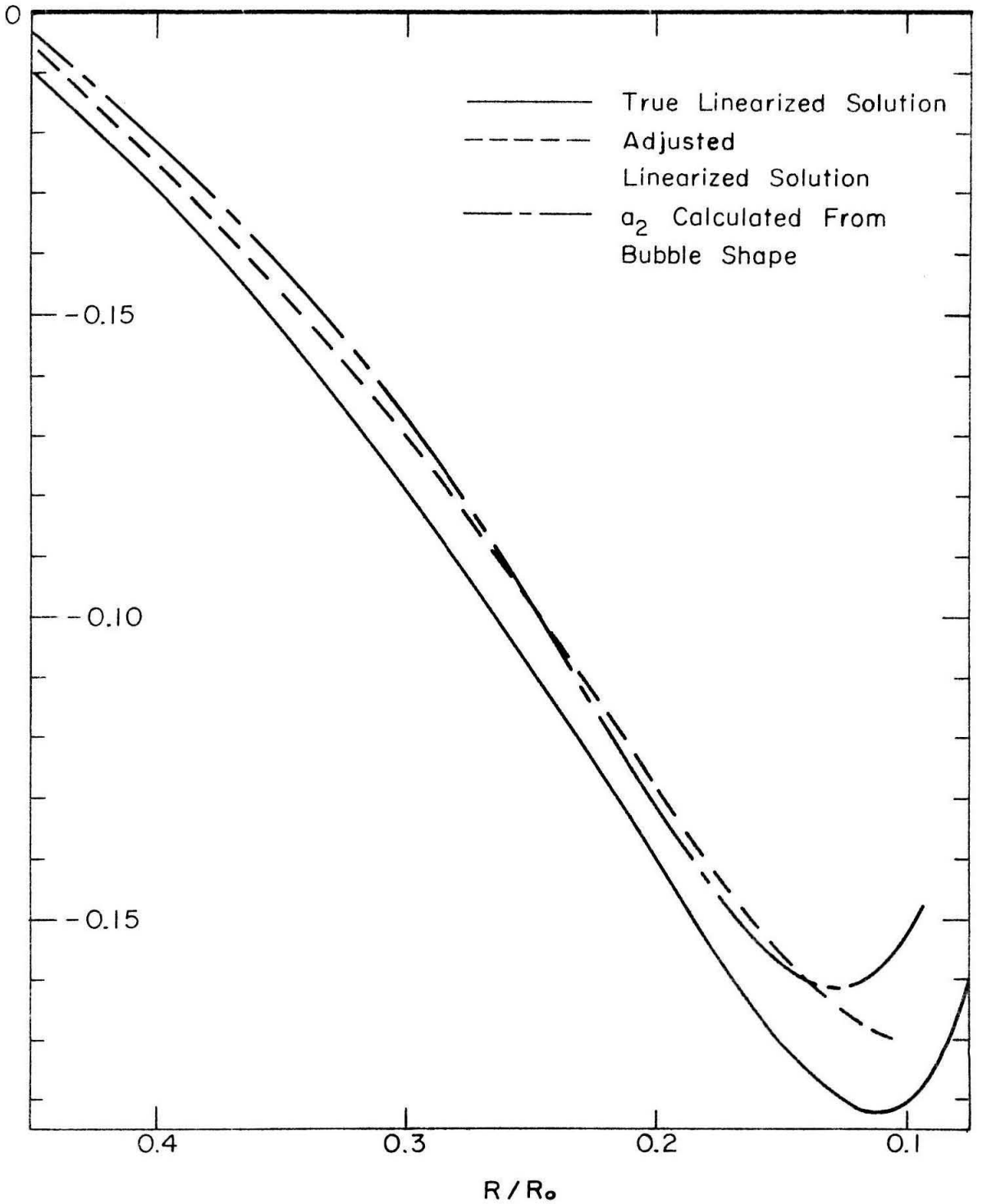

Fig. 20 Adjusted Linearized Solution Based on Finite Time Steps Used in Case 3

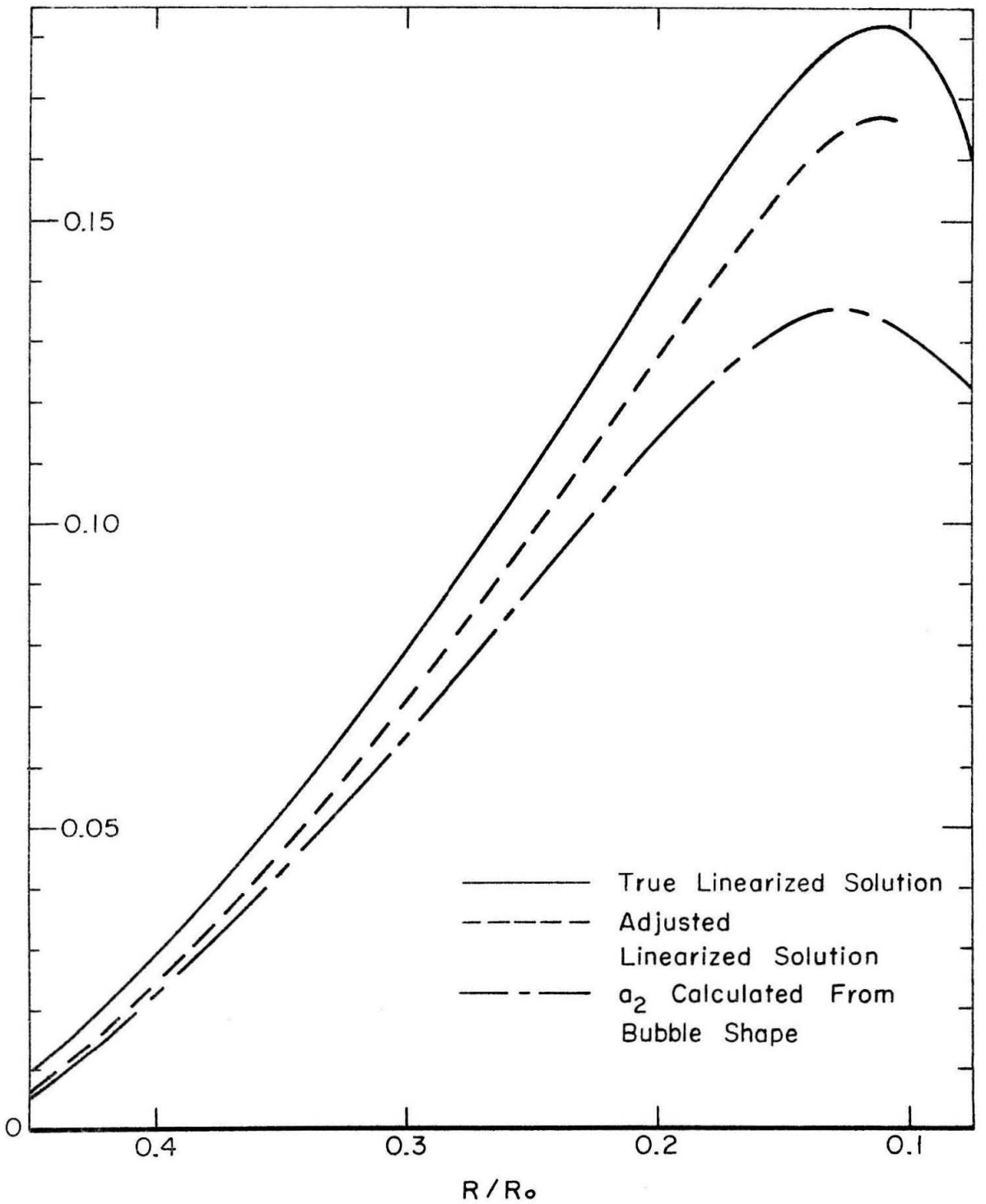

Fig. 21 Adjusted Linearized Solution Based on Finite Time Steps Used in Case 4

a check two different methods were used. First the hypergeometric function from the theory of Plesset and Mitchell was evaluated by summing a complex power series. The second method was to convert the second order differential equation for a_2 into a pair of coupled first order differential equations in $\left(\frac{R}{R_o}\right)$,

$$\frac{Da_2}{D\left(\frac{R}{R_o}\right)} = \left(a_2 - \frac{\frac{9}{2}c}{\sqrt{\left(\frac{R_o}{R}\right)^3 - 1}}\right)\frac{R_o}{R} \qquad \text{(VI-37)}$$

$$\frac{Dc}{D\left(\frac{R}{R_o}\right)} = \left(\frac{2}{3}a_2\sqrt{\left(\frac{R_o}{R}\right)^3 - 1} - 3c\right)\frac{R_o}{R} \quad , \qquad \text{(VI-38)}$$

and integrate them using a standard subroutine. Although the two methods gave identical results, the second method was much faster, especially for small values of $\frac{R}{R_o}$. A summation at $R/R_o = 0.08$, for example, requires about 20,000 complex terms to give four place accuracy. A comparison of the true linearized solution for a_2 illustrated in this thesis with the same curve given by Naudé and Ellis[8] reveals a discrepancy for the smaller values of $\frac{R}{R_o}$. Apparently Naudé and Ellis, who used the summation method, did not include enough terms in this region.

B. Stability

Instability is a common problem in flow simulation. Errors that are small when they are introduced can often grow large enough to obscure the results. Hirt[19] observed that a major difficulty in applying the Marker-and-Cell technique to high Reynolds number flows

was the instability caused by "diffusion-like truncation errors" in the finite difference approximations used throughout the liquid. This type of instability can be reduced by increasing the viscosity and using smaller time steps. For the method of simulation used in this thesis it is pertinent to observe that each time step specifies only the condition of the free surface for the next time step; the potential distribution in the liquid itself is used merely as an estimate for the Liebmann method. Since the finite difference approximations in the liquid involve only space variables, they cannot produce diffusion-like errors similar to the ones analyzed by Hirt.

The small errors left on the free surface by the finite difference approximations are carried from one time step to the next and are a possible source of instability. However, these errors, which are the order of a mesh length in size are usually smoothed out by the interpolation between successive time steps. In general a free boundary point does not fall directly on a net line when it is displaced and must be averaged with the adjacent free boundary points. Free boundary points on the axis of symmetry and on the plane of symmetry are exceptions since these points are constrained to follow the same net lines throughout the collapse. Errors are not smoothed out at these points and so remain in the calculations. As might be expected, these errors behave roughly like the small disturbances in the theory of Plesset and Mitchell; they oscillate at a rate corresponding to one of the higher harmonics. Since the instability analyzed by Plesset and Mitchell is mild in nature (increasing like $R^{-\frac{1}{4}}$ as $R \to 0$), it should not be a problem if the errors on the axis and plane of symmetry are kept small.

This type of instability was most evident in Case 2. The small dimple on the axis of symmetry in surfaces D, E, F, and G in Fig. 9 and in Figs. 14 and 15 is caused by it. Most of the error on the axis seemed to be produced whenever the scale of the final net was halved. By keeping the number of these scale changes to a minimum and by using a fairly large value (0.19) of λ_{MIN} in calculating the velocity, this type of error was greatly reduced in Cases 3 and 4.

C. Validity of Assumptions

The numerical procedure used here is based on a set of assumptions listed in Chapter II. Although all of these assumptions are common in spherical bubble studies such as Rayleigh's classic paper, they will be briefly reviewed in light of the nonspherical solutions. For all cases except Case 4 the maximum velocity on a bubble collapsing in water under a pressure difference of one atm. was under 200 m/sec compared to a sound speed of 1500 m/sec in water and 410 m/sec in water vapor. Under these conditions the assumptions of incompressibility and uniform vapor pressure remain acceptable.

For spherical collapse the only viscous stress on the free surface is normal and is equal to $4\mu \frac{\dot{R}}{R}$. The relative effect of viscosity on spherical collapse can be investigated by comparing the total initial energy of the bubble to the viscous loss during collapse;

$$L_V = \text{Viscous Loss} = -4\mu \int_o^{V_o} \frac{\dot{R}}{R}\, dV \qquad \text{(VI-39)}$$

where $V = \frac{4}{3}\pi R^3$. If the effect of viscosity on the collapse is small, this integral may be estimated by assuming that the collapse velocity

is given by Rayleigh's (nonviscous) theory. Since viscosity slows down the collapse, this estimate will be greater than the actual loss. If R(R) is given by Eq. (VI-13) the loss is

$$4\mu \frac{2}{3}\sqrt{\frac{\Delta p}{\rho}} \int_o^{V_o} \left(\frac{3}{4\pi} V\right)^{-\frac{1}{3}} \sqrt{\frac{V_o}{V} - 1}\, dV$$

$$= \frac{8}{3}\mu \sqrt{\frac{\Delta p}{\rho}} \frac{4\pi}{3} R_o^2 \int_o^1 x^{-5/6}\sqrt{1-x}\, dx \quad ,$$

or

$$L_V < 14.6\mu \sqrt{\frac{\Delta p}{\rho}} \frac{4\pi}{3} R_o^2 \quad . \tag{VI-40}$$

The ratio of the viscous energy loss, L_V, to the initial energy of the bubble, $V_o \Delta p$, does not exceed the value

$$\frac{L_V}{V_o \Delta p} < \frac{14.6\mu}{R_o \rho (\Delta p/\rho)^{\frac{1}{2}}} \quad .$$

In the situations usually encountered it follows that the viscous loss is not important. The viscous stresses for the nonspherical cases considered in this thesis are roughly of the same order as in spherical collapse. This can be easily seen in Cases 3 and 4 by using linearized theory to estimate these stresses. By a simple application of linearized theory outlined in Appendix B, the viscous stresses on a surface described by $r_s = R + a_2(t)P_2(\cos\theta) + a_4(t)P_4(\cos\theta)$ are

$$-\sigma_{dd} = 4\mu \frac{\dot{R}}{R} + \mu\left(\frac{8\dot{a}_2}{R} + \frac{4a_2}{R^2}\dot{R}\right)P_2(\cos\theta)$$

$$+ \mu\left(12\frac{\dot{a}_4}{R} + 12a_4\frac{\dot{R}}{R^2}\right)P_4(\cos\theta) \tag{VI-41}$$

and

$$-\sigma_{d\theta} = 6\mu\left(\frac{\dot{a}_2}{R} + 2a_2\frac{\dot{R}}{R^2}\right)\cos\theta\sin\theta$$

$$+ 8\mu\left(\frac{\dot{a}_4}{R} + 2a_4\frac{\dot{R}}{R}\right)\left(\frac{7}{2}\cos^3\theta + \frac{3}{2}\cos\theta\right)\sin\theta \quad . \qquad \text{(VI-42)}$$

From Figs. 18 and 19 it can be seen that $\frac{\dot{a}_2}{R}$, $\frac{\dot{a}_4}{R}$, $\frac{a_2\dot{R}}{R^2}$, and $\frac{a_4\dot{R}}{R^2}$ are of the order of $\frac{\dot{R}}{R}$ or smaller.

For spherical bubbles collapsing in water under a pressure difference of one atm., surface tension effects become important for initial radii less than 10^{-3} cm. Although surface tension was not included in the calculations, the method could be easily adapted to include it. The linearized equations of Plesset[6] include surface tension and can provide a good estimate of its effect on nonspherical collapse.

VII. THE EFFECT OF GRAVITY

Gravitational effects were not included in any of the cases presented in this study. If, however, the bubble is oriented so that axial symmetry will be preserved, gravity or any other pressure field may be imposed by including it in the Bernoulli equation. Then Eq. (III-3) will have the form

$$\Delta\varphi = \left[\frac{(p_\infty(z)-p_v)}{\rho} + \frac{1}{2}v^2\right]\Delta t \quad . \qquad \text{(VII-1)}$$

Another possible application of the method of simulation used in this thesis could be to an initially spherical bubble collapsing under a uniform pressure gradient. To develop some feeling for this type of problem and also to obtain an estimate of the effect of gravity, it is desirable to have a simple perturbation solution for the effect of a pressure gradient on nonspherical collapse. The chief difficulty is that buoyancy causes the bubble to translate along its axis of symmetry with a velocity $u(t)$ which couples the linearized equations. One approach used by Yeh and Yang[20] was to integrate these coupled equations numerically for various situations. In this case, however, it is more suitable to apply a method developed by Penney, Price, and Ward[21] in their investigation of oscillations of gas bubbles formed by underwater explosions. If the buoyant velocity $u(t)$ is assumed to be much smaller than the mean collapse velocity $R(t)$, the higher harmonics uncouple leaving three equations involving $u(t)$, $R(t)$ and the second harmonic.

The equations of Penney, Price, and Ward will be derived in

the more convenient form of the theory of Plesset and Mitchell. The shape of the bubble is described by

$$r_s = R(t) + \sum_{n=2}^{\infty} a_n(t) P_n(\cos\theta) \qquad \text{(VII-2)}$$

where $|a_n| \ll R$. The origin is determined by the requirement that $a_1(t)$ must vanish. The pressure field will be described by

$$p_\infty - p_v = p(z) = p_o - \rho g(z - z_o) \qquad \text{(VII-3)}$$

where the center of the bubble is initially at $z = z_o$. Only cases in which the variation in $p(z)$ over a bubble diameter is small compared to p_o will be considered.

For such cases the buoyant velocity $u(t)$ should be small compared to $\dot{R}$ throughout most of the collapse. Thus there are two small quantities,

$$\left|\frac{a_n}{R}\right| = O(\epsilon) \qquad \text{and} \qquad \left|\frac{u}{\dot{R}}\right| = O(\delta) \quad . \qquad \text{(VII-4)}$$

As in the theory of Plesset and Mitchell only first order terms in ϵ will be retained. It will be seen that first order terms in δ have no effect on the linearized distortions in shape. To have a first order effect $u(t)$ must be large enough so that $\delta^2 = O(\epsilon)$. Terms of order $\delta^3 = O(\epsilon^{3/2})$ and higher must be neglected to uncouple the equations.

The free surface is described by the equation

$$r_s(\theta, t) - d = f(d, \theta, t) = 0 \quad , \qquad \text{(VII-5)}$$

where the (d, θ) coordinates are measured from the origin in the

bubble moving with speed $u(t)$ in the positive z direction. The time derivative in the moving (d, θ) coordinate system is related to the time derivative in the fixed coordinate system by

$$\left(\frac{\partial}{\partial t}\right)_{\text{moving}} = \left(\frac{\partial}{\partial t}\right)_{\text{fixed}} + u(t)\,\frac{\partial}{\partial z}$$

$$= \left(\frac{\partial}{\partial t}\right)_{\text{fixed}} + u(t)\left(\cos\theta\,\frac{\partial}{\partial d} - \frac{\sin\theta}{d}\,\frac{\partial}{\partial \theta}\right) . \qquad \text{(VII-6)}$$

The kinematic free boundary condition is

$$\frac{Df}{Dt} = \left(\frac{\partial f}{\partial t}\right)_{\text{moving}} - u(t)\left(\cos\theta\,\frac{\partial f}{\partial d} - \frac{\sin\theta}{d}\,\frac{\partial f}{\partial \theta}\right)_{d=r_s}$$

$$+\left(v_d\,\frac{\partial f}{\partial d} + \frac{v_\theta}{d}\,\frac{\partial f}{\partial \theta}\right)_{d=r_s} = 0 \quad , \qquad \text{(VII-7)}$$

where v_d and v_θ are the components in the d and θ directions of the velocity relative to the fixed coordinate system. Equations (VII-5) and (VII-7) produce

$$\dot{r}_s = \left(\frac{\partial f}{\partial t}\right)_{\text{moving}} = \left[v_d - u(t)\cos\theta - \frac{1}{r_s}\,(v_\theta + u(t)\sin\theta)\,\frac{\partial r_s}{\partial \theta}\right]_{d=r_s}$$

or

$$\dot{r}_s = (v_d)_{r_s} - u\cos\theta + O(\delta^3) \quad . \qquad \text{(VII-8)}$$

The velocity potential φ outside the bubble can be expanded in the form

$$\varphi = \frac{b_o}{d} + \frac{b_1 \cos\theta}{d^2} + \sum_{n=2}^{\infty} \frac{b_n}{d^{n+1}}\,P_n(\cos\theta) \quad . \qquad \text{(VII-9)}$$

Equations (VII-2) and (VII-8) produce

$$\left(\frac{\partial \varphi}{\partial d}\right)_{r_s} = u\cos\theta + \dot{r}_s$$

$$= \dot{R} + u\cos\theta + \sum_{n=2}^{\infty} \dot{a}_n(t) P_n(\cos\theta) \quad . \tag{VII-10}$$

To first order in ϵ, Eq. (VII-10) is satisfied by

$$\varphi = -\frac{R^2\dot{R}}{d} - \frac{R^3 u}{2d^2}\cos\theta$$

$$-\sum_{n=2}^{\infty} \frac{R^{n+2}}{(n+1)d^{n+1}}\left[\dot{a}_n + 2a_n\frac{\dot{R}}{R}\right] P_n(\cos\theta) + O(\epsilon^{3/2}) \quad . \tag{VII-11}$$

With the aid of Eq. (VII-5) the Bernoulli equation on the free surface may be written as

$$\left(\frac{\partial \varphi}{\partial t}\right)_{r_s} - u\left(\frac{\partial \varphi}{\partial d}\cos\theta - \frac{1}{d}\frac{\partial \varphi}{\partial \theta}\sin\theta\right) + \frac{1}{2}\left(v_d^2 + \left(\frac{v_\theta}{d}\right)^2\right)_{r_s} = \frac{p(z)}{\rho}$$

$$= \frac{p_o}{\rho} - g(z_c - z_o) - g\, r_s \cos\theta \tag{VII-12}$$

where $z_c - z_o$ is the total distance traveled by the moving coordinate system. That is

$$z_c - z_o = \int_o^t u(t)dt \quad . \tag{VII-13}$$

It has been mentioned that the variation in pressure over a bubble diameter, $2\rho g R_o$, must be small compared to p_o. More exactly, it will be seen that

$$\frac{\rho g R}{p_o} < O(\delta) \quad . \tag{VII-14}$$

Thus to first order in ϵ the pressure on the bubble surface is

$$\frac{p(z)}{\rho} = \frac{p_o}{\rho} - g(z_c - z_o) - gR\cos\theta \quad . \qquad \text{(VII-15)}$$

From Eq. (VII-11) the first term of Eq. (VII-12) is to first order in ϵ,

$$\left(\frac{\partial\varphi}{\partial t}\right)_{r_s} = -\frac{1}{R}\frac{d}{dt}(R^2\dot{R}) - \frac{1}{2R^2}\frac{d}{dt}(R^3 u)\cos\theta + \sum_{n=2}^{\infty}\left[\frac{a_n}{R^2}\frac{d}{dt}(R^2\dot{R}) - \frac{\ddot{a}_n}{n+1}R - \frac{n+4}{n+1}\dot{R}\dot{a}_n - 2a_n\frac{\dot{R}^2}{R} - \frac{2a_n}{n+1}\ddot{R}\right]P_n(\cos\theta) + O(\epsilon^{3/2}) \quad . \qquad \text{(VII-16)}$$

Similarly, to first order in ϵ the second term of Eq. (VII-12) is

$$-u\left(v_d\cos\theta - \frac{v_\theta}{d}\sin\theta\right)_{r_s} = -u\left[(\dot{R}+u\cos\theta)\cos\theta - \frac{1}{2}u\sin^2\theta\right] + O(\epsilon^{3/2})$$

$$= -u\dot{R}\cos\theta - u^2\left(\cos^2\theta - \frac{1}{2}\sin^2\theta\right)$$

$$= -u\dot{R}\cos\theta - u^2 P_2(\cos\theta) \quad . \qquad \text{(VII-17)}$$

Finally the third term is to first order in ϵ

$$\frac{1}{2}\left(v_d^2 + \left(\frac{v_\theta}{d}\right)^2\right)_{r_s} = \frac{1}{2}\dot{R}^2 + u\dot{R}\cos\theta + \frac{1}{2}u^2\cos^2\theta + \dot{R}\sum_{n=2}^{\infty}\dot{a}_n P_n(\cos\theta) + \frac{1}{8}u^2\sin^2\theta + O(\epsilon^{3/2})$$

$$= \frac{1}{2}\dot{R}^2 + u\dot{R}\cos\theta + \frac{1}{4}u^2 + \frac{1}{4}u^2 P_2(\cos\theta) + \dot{R}\sum_{n=2}^{\infty}\dot{a}_n P_n(\cos\theta) \quad . \qquad \text{(VII-18)}$$

The equation resulting from the substitution of Eqs. (VII-15) through (VII-18) into Eq. (VII-12) must be independently satisfied by the terms

proportional to each of the Legendre polynomials. The terms constant in θ give

$$R\ddot{R} + \frac{3}{2}\dot{R}^2 + \frac{p_o}{\rho} = \frac{1}{4}u^2 + \rho g \int_o^t u\,dt \quad . \qquad \text{(VII-19)}$$

The terms proportional to $\cos\theta$ give

$$\frac{3}{2}u\dot{R} + \frac{1}{2}R\dot{u} = gR \quad . \qquad \text{(VII-20)}$$

Terms proportional to $P_2(\cos\theta)$ give

$$R\ddot{a}_2 + 3\dot{R}\dot{a}_2 - \ddot{R}a_2 = -\frac{9}{4}u^2 \quad , \qquad \text{(VII-21)}$$

and terms proportional to $P_n(\cos\theta)$ give for $n = 3,4,5\ldots$,

$$R\ddot{a}_n + 3\dot{R}\dot{a}_n - (n-1)\ddot{R}a_n = 0 \quad . \qquad \text{(VII-22)}$$

With a little manipulation Eqs. (VII-19), (VII-20), and (VII-21) can be shown to be equivalent to those of Penny, Price, and Ward except for a term in Eq. (VII-20) which has been neglected in this treatment. Equation (VII-22) is unchanged from ordinary linear theory, but Eq. (VII-21) contains the effect of the buoyant velocity on $a_2(t)$. Eq. (VII-20) may be integrated to give

$$u(t) = \frac{2g}{R^3}\int_o^t R^3\,dt \quad . \qquad \text{(VII-23)}$$

This equation, which was first derived by Herring[22], exactly describes the buoyant motion of a spherical hollow initially at rest. Although u increases like R^{-3} as $R \to 0$, in many cases the asymmetry of the bubble will cause large deformations before u reaches a significant magnitude.

If the effect of the buoyant velocity is small, an estimate of $\int_o^t R^3 dt$ can be made using the Rayleigh solution;

$$\int_o^t R^3(t)dt = \int_{R_o}^{R} \frac{R^3}{\dot{R}}\, dR \qquad \text{(VII-24)}$$

$$= \int_{R_o}^{R} \frac{R^3}{\sqrt{\frac{2}{3}\frac{p_o}{\rho}\left(\frac{R_o^3}{R^3} - 1\right)}}\, dR$$

$$= \frac{1}{3} R_o^4 \sqrt{\frac{3\rho}{2p_o}} \int_{(R/R_o)^3}^{1} \frac{x^{5/6}}{\sqrt{1-x}}\, dx \quad . \qquad \text{(VII-25)}$$

The integral

$$I(\alpha) \equiv \int_{\alpha}^{1} \frac{x^{5/6}}{\sqrt{1-x}}\, dx \qquad 1 \geqslant \alpha \geqslant 0 \qquad \text{(VII-26)}$$

can be expressed as an incomplete beta-function:

$$I(\alpha) = B\left(\frac{11}{6}, \frac{1}{2}\right) - B_\alpha\left(\frac{11}{6}, \frac{1}{2}\right) \qquad \text{(VII-27)}$$

where

$$B(p,q) \equiv \int_o^1 x^{p-1}(1-x)^{q-1}\, dx = \frac{\Gamma(p)\Gamma(q)}{\Gamma(p+q)}$$

and

$$B_\alpha(p,q) \equiv \int_o^\alpha x^{p-1}(1-x)^{q-1} dx \quad .$$

It is more convenient, however, to express $I(\alpha)$ as an expansion in powers of $(1-\alpha)$. The integral may be rewritten as

$$I(\alpha) = \int_\alpha^1 \frac{x(1-(1-x)^{-1/6}}{\sqrt{1-x}}\, dx = \int_\alpha^1 \frac{x}{\sqrt{1-x}}\left(\sum_{n=o}^{\infty} d_n(1-x)^n\right) dx \qquad \text{(VII-28)}$$

where $d_o = 1$ and $d_n = \frac{\frac{1}{6}\cdot\frac{11}{6}\cdots(n-5/6)}{n!} > 0$. The recursion relation connecting coefficients is

$$d_n = \frac{n-5/6}{n}\, d_{n-1} \qquad n = 1, 2, 3, \ldots \quad \text{(VII-29)}$$

For any $\alpha > 0$,

$$I(\alpha) = \sum_{n=o}^{\infty} d_n \int_{\alpha}^{1} x(1-x)^{n-1/2}\, dx$$

$$= \sum_{n=o}^{\infty} d_n \int_{1-\alpha}^{o} (v-1)v^{n-1/2}\, dv \qquad \text{(where } v = 1-x\text{)}$$

$$= -\sum_{n=o}^{\infty} d_n \left(\frac{(1-\alpha)^{n+3/2}}{n+3/2} - \frac{(1-\alpha)^{n+1/2}}{n+1/2} \right)$$

$$= \sum_{n=o}^{\infty} 2d_n (1-\alpha)^{n+1/2} \left(\frac{1}{2n+1} - \frac{(1-\alpha)}{2n+3} \right)$$

$$= 2(1-\alpha)^{1/2} + \sum_{n=1}^{\infty} \frac{2(d_n - d_{n-1})}{2n+1} (1-\alpha)^{n+1/2} \,. \quad \text{(VII-30)}$$

A further simplification in Eq. (VII-20) can be made using the recursion relation (VII-29);

$$I(\alpha) = (1-\alpha)^{\frac{1}{2}} \left(2 - \frac{5}{3} \sum_{n=o}^{\infty} \frac{d_n}{(n+1)(2n+3)} (1-\alpha)^{n+1} \right)$$

$$= (1-\alpha)^{\frac{1}{2}} \left(2 - \frac{5}{9}(1-\alpha) - \frac{1}{36}(1-\alpha)^2 - \frac{5}{648}(1-\alpha)^3 - \ldots \right). \quad \text{(VII-31)}$$

The power series $\sum_{n=o}^{\infty} \frac{d_n}{(n+1)(2n+3)} (1-\alpha)^{n+1}$ contains only positive coefficients and converges in the limiting case $\alpha = 0$. Since convergence is slowest at $\alpha = 0$, the error from truncating the series will be greatest there. Define the truncated solution,

$$I_N \equiv (1-\alpha)\left(2 - \frac{5}{3}\sum_{n=o}^{N} \frac{d_n(1-\alpha)^{n+1}}{(n+1)(2n+3)}\right) , \qquad \text{(VII-32)}$$

and error ,

$$E_N(\alpha) \equiv \frac{I_N(\alpha)-I(\alpha)}{I(\alpha)} . \qquad \text{(VII-33)}$$

The value of $I(0)$ calculated from the tabulated gamma functions is 1.4003. Values of $I_N(0)$ and $E_N(0)$ are listed in Table IX.

TABLE IX

Truncated Solution and Error for $\alpha = 0$

N	0	1	2	3
$I_N(0)$	1.4444	1.4167	1.4089	1.4057
$E_N(0)$	0.0315	0.0117	0.0061	0.0039

Thus

$$I_1(\alpha) = \sqrt{1-\alpha}\left(2 - \frac{5}{9}(1-\alpha) - \frac{1}{36}(1-\alpha)^2\right) \qquad \text{(VII-34)}$$

gives a maximum error of about one percent.

Equations (VII-23), (VII-25), and (VII-34) combine to produce an approximate solution for u(R),

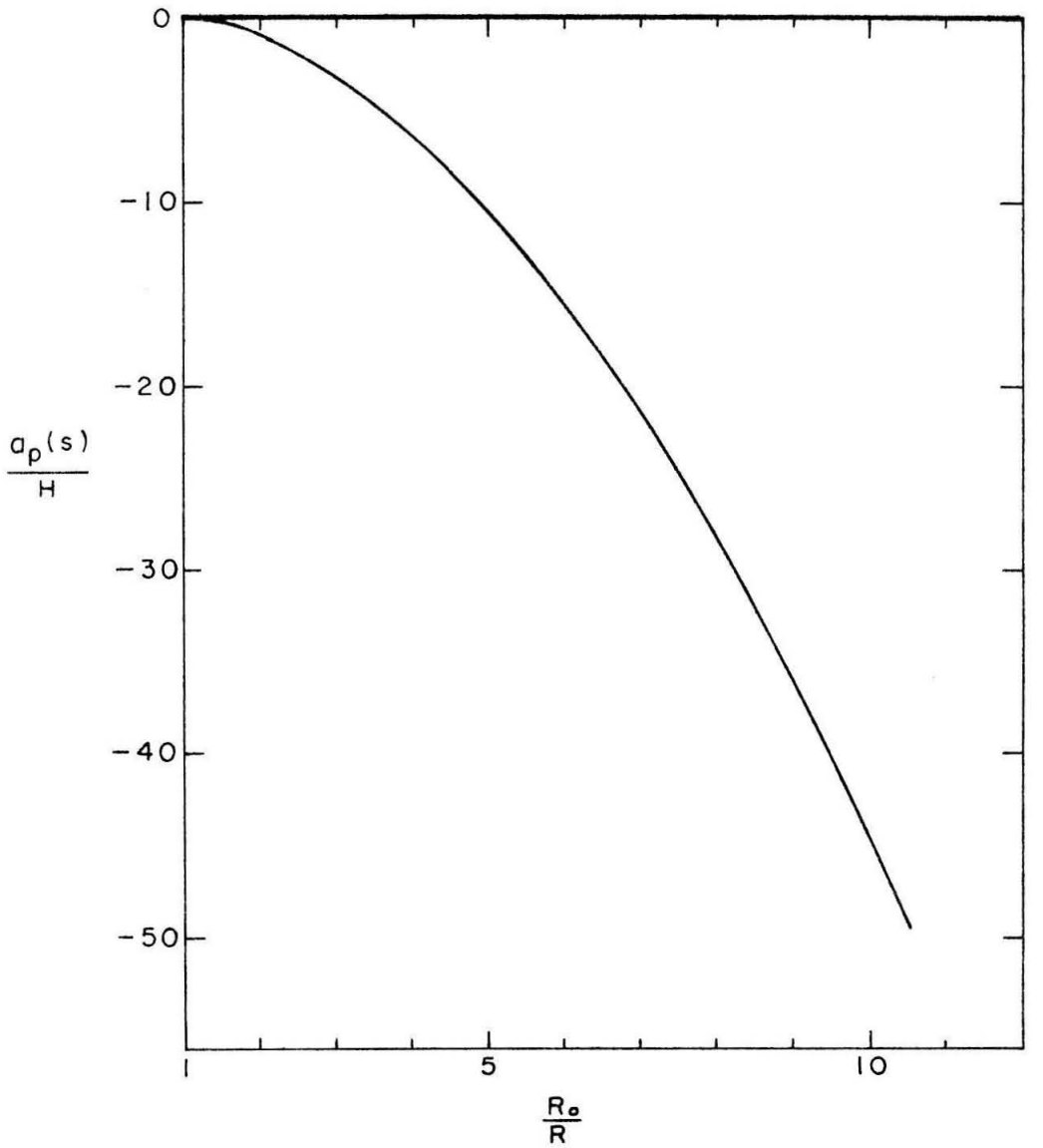

Fig. 22 Distortion of a Collapsing Bubble Caused by a Pressure Gradient

$$u(R) = \frac{2}{3}\frac{gR_o^4}{R^3}\sqrt{\frac{3}{2}\frac{\rho}{p}}\sqrt{1-(R/R_o)^3}\left[2 - \frac{5}{9}\left(1-(R/R_o)^3\right) - \frac{1}{36}\left(1-(R/R_o)^3\right)^2\right] . \qquad \text{(VII-35)}$$

This solution may be applied to Eq. (VII-21). It is consistent with previous approximations to use Rayleigh's solution in the left side of Eq. (VII-21) to eliminate t as an independent variable with the result

$$\frac{2p_o}{3\rho R_o}\left[s^{-2}(1-s^3)\frac{d^2a_2}{ds^2} + \left(\frac{3}{2}s^{-3} - 3\right)\frac{da_2}{ds} + \frac{3}{2}s^{-4}a_2\right] = -\frac{9}{4}u^2 \qquad \text{(VII-36)}$$

where $s \equiv R/R_o$. Application of Eq. (VII-35) produces

$$s^4(1-s^3)\frac{d^2a_2}{ds^2} + \left(\frac{3}{2} - 3s^3\right)s^3\frac{da_2}{ds} + \frac{3}{2}s^2a_2 = -R_o\left(\frac{gR_o}{\frac{2p_o}{3\rho}}\right)^2(1-s^3)\left[2 - \frac{5}{9}(1-s^3) - \frac{1}{36}(1-s^3)^2\right]^2 . \qquad \text{(VII-37)}$$

The general solution of Eq. (VII-37) consists of Plesset and Mitchell's solution of the homogeneous equation added to a gravity induced particular solution $a_p(s)$ satisfying the homogeneous initial conditions

$$a_p(1) = 0 \quad \text{and} \quad \dot{a}_p(1) = 0 . \qquad \text{(VII-38)}$$

The function $a_p(s)/H$ where $H = R_o\left(\frac{3\rho g R_o}{2p}\right)^2$ was calculated by numerical integration of Eq. (VII-37) and is plotted in Fig. 22.

Consider Eq. (VII-35) again. Combining it with Eq. (VII-24) produces an estimate for the ratio of the buoyant velocity to the mean collapse velocity,

$$\frac{u}{\dot{R}} = - \frac{\rho g R_o}{p_o} \left(\frac{R_o}{R}\right)^{3/2} \left[2 - \frac{5}{9} \left(1-(R/R_o)^3\right) - \frac{1}{36} \left(1-(R/R_o)^3\right)^2 \right] . \qquad \text{(VII-39)}$$

Equation (VII-14) may be deduced from this relationship. According to this estimate,

$$\left(\frac{u}{\dot{R}}\right)^2 \to 2.0 \left(\frac{\rho g R_o}{p_o}\right) \left(\frac{R_o}{R}\right)^3 \quad \text{as} \quad R/R_o \to 0 \quad . \qquad \text{(VII-40)}$$

Unless $\left(\frac{u}{\dot{R}}\right)^2$ is of order $\epsilon = \sum_n |a_n|$ for nonspherical collapse, the effect of buoyancy will be unimportant. Even for a bubble radius initially as large as one cm in water under atmospheric pressure, gravity gives $\left(\frac{u}{\dot{R}}\right)^2 = O(10^{-6})$ when the bubble has shrunk to one tenth of its initial radius. Under ordinary conditions gravity is not significant for the range of bubble sizes of interest in cavitation.

APPENDIX A

Garabedian's Estimate of the Relaxation Factor Applied to the Axially Symmetric Case

To show that Garabedian's[16] analysis is formally unchanged in the axially symmetric case, his derivation will be given while adapting it to the axially symmetric situation. The value of the potential during the n'th Liebmann iteration at the nodal point $r = ih$, $z = jh$ will be referred to as φ^n_{ij}. The Liebmann method with overrelaxation applied to Eq. (III-5) can be described by

$$4(\varphi^{n+1}_{i,j} - \varphi^{n}_{i,j}) = \alpha\left(\varphi^{n+1}_{i,j-1} + \varphi^{n+1}_{i-1,j}\left(1 - \frac{h}{2r}\right)\right.$$

$$\left. + \varphi^{n}_{i,j+1} + \varphi^{n}_{i+1,j}\left(1 + \frac{h}{2r}\right) - 4\varphi^{n}_{i,j}\right) \quad . \tag{A-1}$$

This equation may be rearranged in the form

$$\frac{1}{h^2}\left(\varphi^{n}_{i,j-1} + \varphi^{n}_{i-1,j}\left(1 - \frac{h}{2r}\right) + \varphi^{n}_{i,j+1} + \varphi^{n}_{i+1,j}\left(1 + \frac{h}{2r}\right) - 4\varphi_{i,j}\right)$$

$$= \frac{1}{h^2}\left(\varphi^{n+1}_{i,j} - \varphi^{n}_{i,j} - \varphi^{n+1}_{i-1,j} + \varphi^{n}_{i-1,j}\right)$$

$$+ \frac{1}{h^2}\left(\varphi^{n+1}_{i,j} - \varphi^{n}_{i,j} - \varphi^{n+1}_{i,j-1} + \varphi^{n}_{i,j-1}\right)$$

$$+ \frac{1}{2rh}\left(\varphi^{n+1}_{i-1,j} - \varphi^{n}_{i-1,j}\right) + \frac{2C}{h}\left(\varphi^{n+1}_{i,j} - \varphi^{n}_{i,j}\right) \tag{A-2}$$

where C is specified by Eq. (III-16).

The n index is assumed to correspond to a time-like variable τ which increases by a value of h with each Liebmann iteration. For small values of h Eq. (B-2) is equivalent to the partial differential equation

$$\varphi_{rr} + \frac{1}{r}\varphi_r + \varphi_{zz} = \varphi_{r\tau} + \varphi_{z\tau} + \frac{1}{2r}\varphi_\tau + 2C\varphi_\tau \quad . \tag{A-3}$$

The substitution $s = \tau + \frac{r}{2} + \frac{z}{2}$ is used to produce the canonical form

$$\nabla^2\varphi = \frac{1}{2}\varphi_{ss} + 2C\varphi_s \quad . \tag{A-4}$$

Equation (A-4) is formally identical to Garabedian's equation for the plane case. Separation of variables leads to Garabedian's result that

$$\varphi = \varphi_o(r,z) + \sum_{n=1}^{\infty} [a_n \exp(-q_n s) + b_n(-q_n's)]U_n(r,z) \tag{A-5}$$

where q_n amd q'_n are related to the n'th eigenvalue of Eq. (III-17) by

$$q_n = 2C - \sqrt{4C^2 - 2k_n^2} \quad \text{and} \quad q'_n = 2C + \sqrt{4C^2 - 2k_n^2} \quad . \tag{A-6}$$

The function $\varphi_o(r,z)$ represents the solution of Laplace's equation and the added terms in Eq. (A-5) represent the error. The term in the error containing q_1 decreases at the slowest rate. As N the number of Liebmann iterations increases, this term decreases like exp(-qNh) where q is defined by Eq. (III-15).

APPENDIX B

An Estimate of the Viscous Stresses on a Nonspherical Bubble

Although linearized theory neglects viscosity, it can be used to estimate the viscous stress if the effect of viscosity on the flow is small. Linearized theory[6] states that a bubble described by a radius of

$$r_s = R_o + a_2 P_2(\cos\theta) + a_4 P_4(\cos\theta) \quad \text{where} \quad \left|\frac{a_n}{R}\right| = O(\epsilon) \tag{B-1}$$

has the velocity potential

$$\varphi = -\frac{R^2\dot{R}}{d} - \frac{R^4}{3d^3}\left(\dot{a}_2 + 2a_2\frac{\dot{R}}{R}\right)P_2(\cos\theta)$$
$$-\frac{R^6}{5d^5}\left(\dot{a}_4 + 2a_4\frac{\dot{R}}{R}\right)P_4(\cos\theta) \quad . \tag{B-2}$$

The two components of the velocity are

$$v_d = \frac{\partial\varphi}{\partial d} = \frac{R^2\dot{R}}{d^2} + \frac{R^4}{d^4}\left(\dot{a}_2 + 2a_2\frac{\dot{R}}{R}\right)P_2(\cos\theta)$$
$$+\frac{R^6}{d^6}\left(\dot{a}_4 + 2a_4\frac{\dot{R}}{R}\right)P_4(\cos\theta) \tag{B-3}$$

$$v_\theta = \frac{1}{d}\frac{\partial\varphi}{\partial\theta} = \frac{R^4}{d^4}\left(\dot{a}_2 + 2a_2\frac{\dot{R}}{R}\right)\cos\theta\,\sin\theta$$
$$+\frac{R^6}{d^6}\left(\dot{a}_4 + 2a_4\frac{\dot{R}}{R}\right)\left(\frac{7}{2}\cos^3\theta + \frac{3}{2}\cos\theta\right)\sin\theta \quad . \tag{B-4}$$

For the axially symmetric case the two nonzero elements of the stress tensor in spherical coordinates[22] are

$$-\sigma_{dd} = -2\mu\frac{\partial v_d}{\partial d} \tag{B-5}$$

and

$$-\sigma_{d\theta} = -\mu\left(\frac{1}{d}\frac{\partial v_d}{\partial\theta} + \frac{\partial v_\theta}{\partial d} - \frac{v_\theta}{d}\right) . \qquad \text{(B-6)}$$

To first order in ϵ the values of these elements on the free surface are

$$\begin{aligned} -\sigma_{dd} &= 2\mu\left(2\frac{\dot{R}R^2}{r_s^2} + 4\frac{R^4}{r_s^5}\left(\dot{a}_2 + 2a_2\frac{\dot{R}}{R}\right)P_2(\cos\theta)\right. \\ &\quad \left. + 6\frac{R^6}{r_s^7}\left(\dot{a}_4 + 2a_4\frac{\dot{R}}{R}\right)P_4(\cos\theta)\right) \\ &= 4\mu\frac{\dot{R}}{R} + \mu\left(8\frac{\dot{a}_2}{R} + 4a_2\frac{\dot{R}}{R^2}\right)P_2(\cos\theta) \\ &\quad + \mu\left(12\frac{\dot{a}_4}{R} + 12a_4\frac{\dot{R}}{R^2}\right)P_4(\cos\theta) \end{aligned} \qquad \text{(B-7)}$$

and

$$\begin{aligned} -\sigma_{d\theta} &= \left(\frac{\mu}{R} + \frac{4\mu}{R} + \frac{\mu}{R}\right)\left(\dot{a}_2 + 2a_2\frac{\dot{R}}{R}\right)\cos\theta\sin\theta \\ &\quad + \left(\frac{\mu}{R} + \frac{6\mu}{R} + \frac{\mu}{R}\right)\left(\dot{a}_4 + 2a_4\frac{\dot{R}}{R}\right)\left(\frac{7}{2}\cos^3\theta + \frac{3}{2}\cos\theta\right)\sin\theta \\ &= 6\mu\left(\frac{\dot{a}_2}{R} + 2a_2\frac{\dot{R}}{R^2}\right)\cos\theta\sin\theta \\ &\quad + 8\mu\left(\frac{\dot{a}_4}{R} + 2a_4\frac{\dot{R}}{R^2}\right)\left(\frac{7}{2}\cos^3\theta + \frac{3}{2}\cos\theta\right)\sin\theta \quad . \end{aligned} \qquad \text{(B-8)}$$

REFERENCES

[1] Lord Rayleigh, "On the Pressure Developed in a Liquid During the Collapse of a Spherical Cavity", Phil. Mag. 34, 94 (1917).

[2] M. Kornfeld and L. Suvorov, "On the Destructive Action of Cavitation", J. Appl. Phys. 15, 495 (1944).

[3] M. Rattray, "Perturbation Effects in Cavitation Bubble Dynamics", Ph. D. thesis, California Institute of Technology, (1951).

[4] M. S. Plesset, "Shockwaves from Cavity Collapse", Phil. Trans. Roy. Soc. London A 260, 241 (1966).

[5] T. B. Benjamin and A. T. Ellis, "The Collapse of Cavitation Bubbles and the Pressures Thereby Produced Against Solid Boundaries", Phil. Trans. Roy. Soc. London A 260, 221 (1966).

[6] M. S. Plesset, "On the Stability of Fluid Flows with Spherical Symmetry", J. Appl. Phys. 25, 96 (1953).

[7] M. S. Plesset and T. P. Mitchell, "On the Stability of the Spherical Shape of a Vapor Cavity in a Liquid", Quart. Appl. Math. 13 (1956).

[8] C. F. Naudé and A. T. Ellis, "On the Mechanism of Cavitation Damage by Nonhemispherical Cavities Collapsing in Contact with a Solid Boundary", Trans. Am. Soc. Mech. Engrs., J. Basic Eng. 83, 648 (1961).

[9] N. D. Shutler and R. B. Mesler, "A Photographic Study of the Dynamics and Damage Capabilities of Bubbles Collapsing Near Solid Boundaries", Trans. Am. Soc. Mech. Engrs., J. Basic Eng. 87, 511 (1965).

[10] T. M. Mitchell, C. L. Kling, R. Cheesewright, F. G. Hammitt, "Numerical and Photographic Studies of Asymmetric Bubble Collapse", U. of Michigan, College of Eng. Report 07738-5-T (1967).

[11] J. E. Welch, F. H. Harlow, J. P. Shannon, and B. J. Daly, "The MAC Method-A Computing Technique for Solving Viscous, Incompressible, Transient Fluid-Flow Problems Involving Free Surfaces", U. of Calif., Los Alamos, N. Mex. Report LA-3425 (1965).

[12] R. Chan, R. Street, and T. Strelkoff, "Computer Studies of Finite-Amplitude Water Waves", Dept. of Civil Eng., Stanford Univ. Report 104 (1969).

[13] F. R. Gilmore, "The Growth or Collapse of a Spherical Bubble in a Viscous Compressible Liquid", Hydrodynamics Lab., California Institute of Technology, Report 26-4 (1952).

[14] F. S. Shaw, An Introduction to Relaxation Methods (Dover Publications, New York, 1953), Chap. VI.

[15] S. Frankel, "Convergence Rates of Iterative Treatments of Partial Differential Equations", Mathematical Tables and Other Aids to Computation IV, 65 (1950).

[16] P. R. Garabedian, "Estimation of the Relaxation Factor for Small Mesh Size", Mathematical Tables and Other Aids to Computation X, 183 (1956).

[17] G. H. Shortley and R. Weller, "The Numerical Solution of Laplace's Equation", J. Appl. Phys. 9, 334 (1938).

[18] N. L. Hancox and J. H. Brunton, "The Erosion of Solids by the Repeated Impact of Liquids", Phil. Trans. Roy. Soc. London A 260, 121 (1966).

[19] C. W. Hirt, "Heuristic Stability Theory for Finite Difference Equations", J. Computational Physics, 2, 339 (1968).

[20] H. C. Yeh and W. J. Yang, "Dynamics of Bubbles Moving in Liquids with Pressure Gradient", J. Appl. Phys. 39, 3156 (1968).

[21] W. G. Penney and A. G. Price, Unpublished Results, A. B. Ward, Unpublished Results, described in R. H. Cole Underwater Explosions (Princeton University Press 1948), p. 310.

[22] C. Herring, "Theory of the Pulsations of the Gas Bubble Produced by an Underwater Explosion", U. S. National Defense Research Committee Report (1941), described in The Scientific Papers of Sir Geoffrey Ingram Taylor (Cambridge University Press 1963), Vol III, p.321 and in R. H. Cole Underwater Explosions (Princeton University Press 1948), p. 308.

[23] L. D. Landau and E. M. Lifshitz, Fluid Mechanics (Addison-Wesley Publishing Company Inc., 1959) p. 52.